Technische Universiteit
Eindhoven
University of Technology

Systems and Control
Internship Report
DC 2016.XXX

Modeling and Control of the Underactuated Butterfly Robot

Author:

Fahim Shakib
0829988
m.f.shakib@student.tue.nl

Project Supervisor:

prof. dr. H. Nijmeijer
Department of Mechanical Engineering
Section Dynamics and Control
Eindhoven University of Technology

Advisor:

prof. dr. A. Shiriaev
Department of Engineering Cybernetics
Norwegian University of Science and Technology

Eindhoven, November 2016

Department of Mechanical Engineering
Section Dynamics and Control
Eindhoven University of Technology
PO Box 513
5600 MB Eindhoven
The Netherlands

Abstract

Modeling and Control of the Underactuated Butterfly Robot

In this report a case study on the Butterfly Robot (BR) is performed. The BR is a benchmark setup intended for educational purposes. It consists of two identical figure-eight-shaped plates rigidly placed parallel to each other. The aim is to let a ball roll continuously in one direction on the plates' edge, by controlling the actuator attached to the center of mass of the plates. During this motion, the ball has to stay on the edge of the plates. Feedback is provided by means of a camera measuring the position of the ball and an encoder sensing the orientation of the plates. Since there is no setup available, the results in this report are merely based on simulations.

After introducing a convenient coordinate set, the model of the BR is derived in both excessive and generalized coordinates using a Lagrange approach. The model in generalized coordinates has a lower state dimension and is therefore further used for motion planning and feedback stabilization. The model in excessive coordinates gives insight in the constraint forces. This model is used to see whether the planned motion satisfies the constraints and thus results in a feasible motion. Both models are validated by means of simulations.

After imposing a class of virtual holonomic constraint between the degrees of freedom (DOF) of the system, the dynamics can be written in only one DOF. These dynamics are called the reduced dynamics. The class of virtual holonomic constraints is parametrized by two constants. The phase portrait of the zero dynamics of the reduced dynamics are considered to find feasible trajectories. This results into suitable parameters defining the virtual relation. A consideration from a practical point of view is to keep the angular velocities low, since this is be beneficial for visual feedback. The zero dynamics appear to be unstable and need to be stabilized by means of feedback stabilization.

A feedback law is derived which allows for partial feedback linearization. The dynamics of the system are rewritten to a set of coordinates for which the first coordinate is a scalar representing the position on the periodic motion, and the other coordinates defining the distance to the periodic motion. These dynamics are called transverse dynamics, since they vanish when the actual trajectory is on the desired trajectory. The transverse dynamics are linearized in the vicinity of the planned motion. The resulted system is in the class linear time-varying. The controllability Gramian matrix is considered to prove controllability. An LQR approach is used to compute a stabilizing control law. This involves solving a Periodic Differential Riccati Equation, which is performed using a Convex Optimization approach. Another approach to design a stabilizing state feedback controller uses the notion of Periodic Lyapunov functions. However, due to time consideration, the work on the Periodic Lyapunov functions is unfinished. Stability of the controlled BR is proven by means of the Floquet Theory.

Using simulation in excessive coordinate, it is shown that the controlled BR is able to perform the task of continuous one-directional rolling of the ball when starting on the designed trajectory. Furthermore, a region of attraction is presented visually, which shows that the BR is capable of converging to the designed trajectory up to a certain level of deviations. Here, it is also observed that the region of attraction contracts and expands for different positions on the periodic motion. Another result is that the BR is able to start from a zero velocity and position, which is convenient for conducting experiments.

Contents

Chapter 1

Introduction

In daily life, humans perform a lot of prehensile manipulation tasks using their hands. Hands are used to grab objects, hold them tight and move them to a new location. However, humans also manipulate objects in many different ways not involving grasping. A few examples are rolling, sliding, throwing and pushing. A classic example of a non-prehensile task is balancing a ball on the back of the hand. These kind of tasks are often avoided by the design, where there seem to be a preference for grasping. This is due to the complexity of the problem. An example of a non-prehensile task which is unavoidable for human like robots is the task of walking on two legs.

In this report a case study on the Butterfly Robot (BR) is performed. The butterfly robot is a benchmark setup intended for educational purposes, which was introduced by [1]. It consists of two identical figure-eight-shaped plates rigidly placed parallel to each other, see Figure 1.1. An actuator is attached to the center of mass of the plates. Feedback is provided by means of camera measuring the position of the ball and an encoder measuring the orientation of the plates.

The task of the BR is to let a ball roll continuously in one direction on the plates' edges, which is a periodic motion. In control, stabilizing a periodic motion can be considered as a difficult task and requires different tools than for example stabilizing an equilibrium. Another difficulty is that the ball can not be directly manipulated. The frame should be actuated as such that the ball performs the desired motion. Hereto, it should be considered that the ball should not depart from the frame it is supported by.

The design of calculating a control law which allows the robot to perform the non-prehensile task can, roughly spoken, be divided into two parts. The first part concerns the planning of the motion. In this part, insight in and experience with the task is needed. This part is considered as the more difficult part. The second part includes the calculation of a stabilization controller for the planned motion. This part reduces after introducing an efficient computational algorithm, to running a piece of Matlab code.

The work of previous students includes, [2], who worked mainly on motion planning, [3], who worked mainly on orbital stabilization, and, [4], who has contributed mostly on small perturbations on the dynamical model. Their work is used a foundation to the work presented in this report.

The remainder of this report is organized as follows. Chapter 2 provides the choice of the coordinates system and the derivation of the equations of motion. The procedure applied in motion planning is treated in Chapter 3. In Chapter 4, the steps in feedback stabilization are given. A numerical evaluation of the controlled BR is given in Chapter 5. Chapter 6 gives the Conclusions and Recommendations. It should be noted that the applied procedures in motion planning, Chapter 3, and orbital stabilization, Chapter 4, are, in general, taken from [5] and [6].

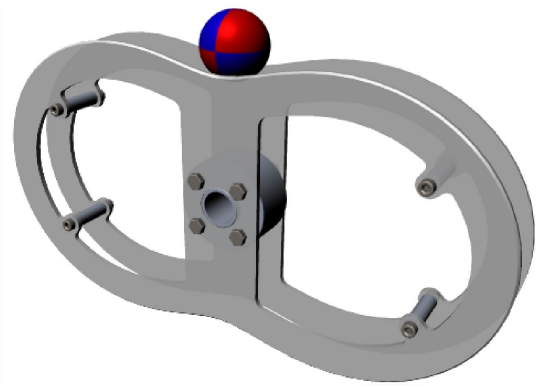

FIGURE 1.1: The Butterfly Robot consisting of a ball rolling on the edge of two identical plates. The plates are aligned on a fixed distance and actuated in the center of mass.

Chapter 2

Modeling of the Butterfly Robot

In order to be able to control the BR, an analytical model should be derived. This chapter introduces first a convenient coordinate system describing the state of the model. Using an Euler-Lagrangian method, the equation of motion for the BR are derived in case of excessive and generalized coordinates. Furthermore, this model is verified by means of simulations.

2.1 Coordinate System

As mentioned in the introduction, the BR consist of two rigid bodies. One of the bodies is the ball, which is supported by the second rigid body, which consists of two parallel eight-shaped plates placed on a fixed distance of each other. The geometrical center of the plates is attached to an actuated rotating axis.

It is assumed that the plates are identical and perfectly aligned such that the dynamics can be written in 2 dimensions. The Grübler count says each rigid body in a 2 dimensional space has 3 degrees of freedom (DOF), namely 2 translational and 1 rotational DOF. Using the Grübler count, it can be concluded that this system has $2 \times 3 = 6$ DOF. Since the rotating axis is fixed in both translational directions, two constraints on position level are imposed. This leaves only 4 DOF for the entire system.

One way to express the state of the BR is to introduce a right-handed inertial frame $\vec{e}^0$ and express the position of the plates and the ball as (x^i, y^i) and the orientation as $\theta^i, i = 1, 2$ respectively. The body-fixed frames $\vec{e}^i, i = 1, 2$ can be introduced attached to the center of mass of the plates and the ball respectively. This coordinate system is schematically shown in Figure 2.1. Note that here it is chosen to impose $(x^1, y^1) = (0, 0)$ in order to let the origin of $\vec{e}^0$ coincide with $\vec{e}^1$.

As mentioned previously, the ball is not rigidly attached to the frame. This results in the following configurations:

1. The ball departs from the plates. In this configuration, the ball's motion is independent of the motion of the plates.
2. The ball is supported by the plates by only one single contact point (on each of the two plates). This is considered as the ideal situation. The ball will rotate on the plates at an effective radius $R = \sqrt{R_b^2 - \left(\frac{d}{2}\right)^2}$, here R_b is the actual radius of the ball and d is the distance between the two plates.
3. The ball deforms such that there is a line contact between the ball and each of the plates.

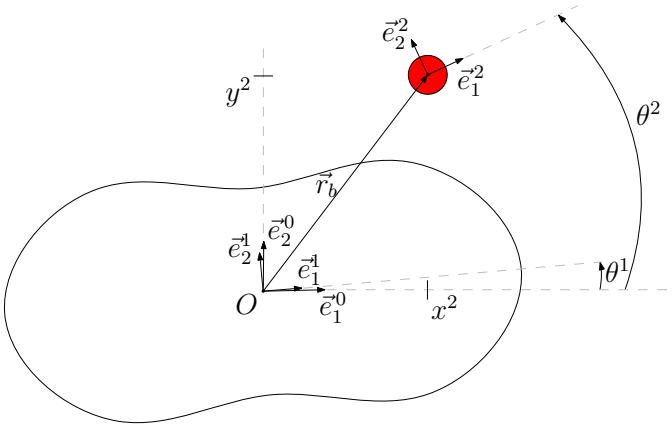

FIGURE 2.1: Coordinate System (x^i, y^i) in $\vec{e}^{\,0}$ with orientations θ^i related to $\vec{e}^{\,0}$ for $i = 1, 2$ for the plates and ball respectively. Note that (x^1, y^1) are omitted in this figure since these coincide with the origin of $\vec{e}^{\,0}$, i.e. $x^1 = y^1 = 0$.

The coordinate set $(x^2, y^2, \theta^1, \theta^2)$ completely describe the position and orientation of the BR. However, they do not directly give insight in the current configuration of the system. Another drawback of this coordinate set is that including interaction between the rigid bodies in the model is a complex modeling task. In order to circumvent these drawbacks, an alternative coordinate system is introduced.

The vector $\vec{\rho}(\varphi)$ evaluated along φ describes the ideal curve of the ball's center of mass when the system is in the ideal configuration, i.e. configuration 2. The angle $\varphi(t)$ is defined as the angle between the position of the ball's center of mass on the ideal curve and the positive $\vec{e}_2^{\,1}$ axis, measured clockwise. For every φ, $\vec{\rho}(\varphi)$ is uniquely defined and, furthermore, $\vec{\rho}(\varphi)$ is periodic over 2π. A Frenet frame is introduced as shown in Figure 2.2, which consists of an unit tangent vector $\vec{\tau}$ and an unit normal vector $\vec{n}$, being orthonormal to each other by definition. The concept is to describe the position of the ball as an offset along the ideal curve $\vec{\rho}(\varphi)$, using the definition

$$\vec{\rho}(\varphi) = \begin{bmatrix} \rho_x(\varphi) & \rho_y(\varphi) \end{bmatrix} \vec{e}^{\,1}.$$

As a first new coordinate, $s(t)$ is introduced representing the arc-length traveled by the center of mass of the ball on the ideal curve $\vec{\rho}$. This coordinate can be expressed in terms of $\vec{\rho}$ as

$$s(\varphi(t)) = \int_0^{\varphi(t)} \left|\left| \frac{\partial \vec{\rho}(\phi(t))}{\partial \phi(t)} \right|\right| d\phi(t).$$

There is an unique relation between $s(\varphi(t))$ and $\vec{\rho}(\varphi)$, which can be used to define the direction of the tangent vector of the Frenet frame as

$$\vec{\tau} = \frac{\partial \vec{\rho}(s(t))}{\partial s(t)} \text{ and } \vec{n} = \vec{\tau} \times \vec{k},$$

with $\vec{k} = \vec{e}_3^{\,0}$. Additionally, the coordinate w is introduced representing the shortest distance between the ball's center of mass and the location on the curve described by $\vec{\rho}$. Note that the shortest distance between the ball's center of mass and the curve described by $\vec{\rho}$ is in the direction of $\vec{n}$. These two coordinates allow to write the position of the ball as

$$\vec{r}_b = \vec{\rho}(s) + w\vec{n},$$

where the vector $\vec{\rho}$ is now parametrized by the coordinate s, i.e. $\vec{\rho} = \vec{\rho}(s)$.

The orientation of the ball with respect to the orientation of the plates can be introduced as the third coordinate $\psi(t)$. The fourth coordinate describing the orientation of the plates with

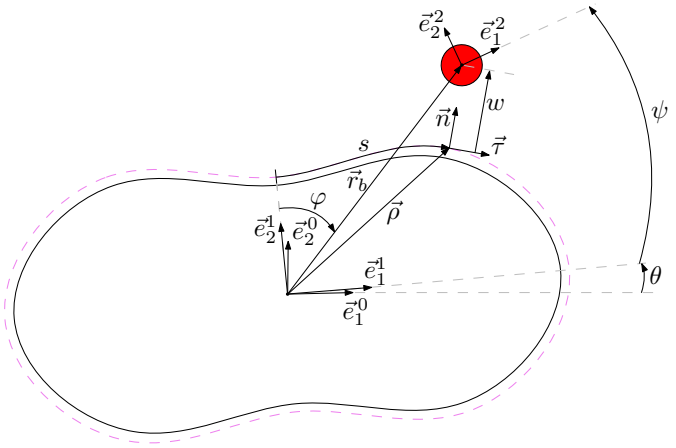

FIGURE 2.2: Coordinate system $(\theta(t), s(t), w(t), \psi(t))$

respect to the inertial frame is kept as $\theta(t)$. See Figure 2.2 for a schematic overview of the new coordinate set.

The coordinates $(\theta(t), s(t), w(t), \psi(t))$ constitute a set which completely describes the position and orientation of the BR. Furthermore, the coordinate $w(t)$ describes the configuration of the BR:

1. $w > 0$ the ball does not contact any of the plates .
2. $w = 0$ the ball is in point contact with each of the plates.
3. $w < 0$ the ball is deformed and is in line contact with each of the plates.

The edge of the plates is defined by

$$r_\delta = \delta(\vartheta) \begin{bmatrix} \sin(\vartheta) & \cos(\vartheta) \end{bmatrix}, \quad \delta(\vartheta) = 0.1095 - 0.0405\cos(2\vartheta), \tag{2.1}$$

with, ϑ being the angle between r_δ and $\vec{e}_2^{\,1}$, measured positive in a clockwise direction. The Frenet frame vectors $\vec{\tau}$ and $\vec{n}$, the ideal curve $\vec{\rho}(\varphi)$, and the traveled distance by the center of mass of the ball s can be found numerically for all φ, using 2.1.

2.2 Equations of Motion in Excessive Coordinates

The approach to derive the equations of motion used here is the Euler-Lagrangian approach. This approach allows deriving the equations of motion without having knowledge about the constraint forces in a system. However, constraint forces can be added to the equations of motion using the theory of Lagrangian multipliers. In this subsection, the equations of motion are derived for the excessive coordinates

$$q(t) = \begin{bmatrix} \theta(t), & s(t), & w(t), & \psi(t) \end{bmatrix}^\top. \tag{2.2}$$

This approach yields the equations of motion as

$$\frac{d}{dt}\frac{\partial L}{\partial \dot{q}} - \frac{\partial L}{\partial q} = Q_{nc}^\top, \tag{2.3}$$

where L is the Lagrangian defined as the kinetic energy T minus the potential energy V, i.e. $L = T - V$. The column of non-conservative forces is represented by

$$Q_{nc} = \begin{bmatrix} u, & 0, & 0, & 0 \end{bmatrix}^\top, \tag{2.4}$$

with u being the torque applied to the center of mass of the plates.

The energy that an object has due to its motion is called kinetic energy. In this case, two types of kinetic energy are relevant, namely translational and rotational kinetic energy. For each rigid body, both types of kinetic energy can be evaluated separately, which allows to write the kinetic energy as a summation of four components. Explicitly, the four components of the kinetic energy are:

- Translational energy of the plates $T_{p,v}$, which equals zero for all times since the plates don't move in the translational direction, i.e.

$$T_{p,v} = 0. \tag{2.5}$$

- Rotational energy of the plates T_{p_ω}, which equals

$$T_{p,\omega} = \frac{1}{2} J_p (\vec{\omega}_p \cdot \vec{\omega}_p), \tag{2.6}$$

  with J_p the mass moment of inertia of the plates with respect to the inertial coordinate frame $\vec{e}^0$, and $\vec{\omega}_p = \dot{\theta}\hat{k}$ being the angular velocity vector.

- Translation energy in the center of mass of the ball $T_{b,v}$, which equals

$$T_{b,v} = \frac{1}{2} m (\vec{v}_b \cdot \vec{v}_b), \tag{2.7}$$

  with m being the mass of the ball and $\vec{v}_b = \frac{d\vec{r}_b}{dt} + \dot{\theta}\hat{k} \times \vec{r}_b$ the velocity of the ball. The term $\dot{\theta}\hat{k} \times \vec{r}_b$ arises in $\vec{v}_b$ due to the velocity of the body-fixed frame $\vec{e}^1$.

- Rotational energy of the ball $T_{b,\omega}$, which equals

$$T_{b,\omega} = \frac{1}{2} J_b (\vec{\omega}_b \cdot \vec{\omega}_b), \tag{2.8}$$

  with J_b the ball's mass moment of inertia about the $\vec{e}_3^2$ axis and $\vec{\omega}_b = \left(\dot{\theta} + \dot{\psi}\right) \hat{k}$ being the angular velocity vector.

The total kinetic energy of the system is

$$T = T_{p,v} + T_{p,\omega} + T_{b,v} + T_{b,\omega}, \tag{2.9}$$

with $T_{p,v}, T_{p,\omega}, T_{b,v}$ and $T_{b,\omega}$ defined in 2.5 to 2.8 respectively.

The potential energy is represented by the gravitational force acting on the center of mass of the ball. The total potential energy is

$$V = m\vec{g} \cdot \left(\Pi(\theta(t)\vec{r}_b\right), \tag{2.10}$$

with

$$\Pi = \begin{bmatrix} \cos(\theta(t)) & -\sin(\theta(t)) \\ \sin(\theta(t)) & \cos(\theta(t)) \end{bmatrix} \text{ and } \vec{g} = \begin{bmatrix} 0, & g, & 0 \end{bmatrix} \vec{e}^0. \tag{2.11}$$

The rotation matrix $\Pi(\theta)$ relates the orientation of the body-fixed frame $\vec{e}^1$ to the inertial frame $\vec{e}^0$, i.e. $\vec{e}^0 = \Pi(\theta)\vec{e}^1$ and $\vec{g}$ represents the vector of gravitational acceleration in the inertial frame.

The Lagrangian of this system is

$$L = T - V, \tag{2.12}$$

with the kinetic energy T given in 2.9 and the potential energy V given in 2.10.

By means of the software package maple, 2.3 is worked out with L defined in 2.12 and Q_{nc} defined in 2.4 for the excessive state $q(t) = \left[\theta(t), \quad s(t), \quad w(t), \quad \psi(t)\right]^\top$. The equations of motion are given in the form

$$M(q)\ddot{q} + C(q,\dot{q})\dot{q} + G(q) = Q_{nc}, \tag{2.13}$$

with the mass matrix

$$M(q) = \begin{bmatrix} (w^2 - 2wx_1 + x_{10})m + J_b + J_p & m(w^2x_2 + wx_6 - w + x_1) & mx_5 & J_b \\ m(w^2x_2 + wx_6 - w + x_1) & m(x_{11}w^2 - 2wx_2 + 1) & 0 & 0 \\ mx_5 & 0 & m & 0 \\ J_b & 0 & 0 & J_b \end{bmatrix}, \tag{2.14}$$

the components of the matrix of the Coriolis and centrifugal forces as

$$C_{1,1} = -m\left(\dot{s}(wx_3 - x_5) + \dot{w}x_1 - w\dot{w}\right), \tag{2.15a}$$

$$C_{1,2} = m\left(\left(-\dot{\theta}w + \dot{s}\right)x_3 + \dot{w}wx_2 + \dot{s}x_4w^2 + wx_7\dot{s} + \dot{\theta}x_5 + x_6\dot{w}\right), \tag{2.15b}$$

$$C_{1,3} = m\left(\dot{s}wx_2 + x_6\dot{s} - x_1\dot{\theta} + \dot{\theta}w\right), \tag{2.15c}$$

$$C_{2,1} = -m\left(-x_3w\dot{\theta} - \dot{w}wx_2 + \dot{\theta}x_5 + \dot{w}\right), \tag{2.15d}$$

$$C_{2,2} = m\left(-\dot{w}x_2 - \dot{s}x_4w + \dot{s}x_9w^2 + \dot{w}wx_{11}\right), \tag{2.15e}$$

$$C_{2,3} = -m\left(\left(-\dot{\theta}w + \dot{s}\right)x_2 - \dot{s}wx_{11} + \dot{\theta}\right), \tag{2.15f}$$

$$C_{3,1} = -m\left(\dot{s}wx_2 - x_1\dot{\theta} + \dot{\theta}w - \dot{s}\right), \tag{2.15g}$$

$$C_{3,2} = m\left(\left(-\dot{\theta}w + \dot{s}\right)x_2 + \dot{s}x_8w + \dot{\theta}\right), \tag{2.15h}$$

$$C_{1,4} = C_{2,4} = C_{3,4} = C_{3,3} = C_{4,1} = C_{4,2} = C_{4,3} = C_{4,4} = 0, \tag{2.15i}$$

and the column containing the gravitational forces as

$$G(q) = m\begin{bmatrix} \vec{g}\cdot(\Pi'(\theta)(\vec{\rho} + w\vec{n})) \\ \vec{g}\cdot\left(\Pi(\theta)(\vec{\tau} + w\vec{\xi})\right) \\ \vec{g}\cdot(\Pi'(\theta)\vec{n}) \\ 0 \end{bmatrix}. \tag{2.16}$$

In these matrices, the derivative of the direction cosine matrix $\Pi(\theta)$ with respect to the angle θ is defined as $\Pi'(\theta) = \frac{\partial}{\partial\theta}\Pi(\theta)$ and the scalars $x_1 \ldots x_{11}$ result from vector products given by

$$x_1 = \vec{\hat{k}}\cdot(\vec{\rho}\times\vec{\tau}), \tag{2.17a}$$

$$x_2 = \vec{\hat{k}}\cdot(\vec{\tau}\times\vec{\kappa}), \tag{2.17b}$$

$$x_3 = \vec{\hat{k}}\cdot(\vec{\rho}\times\vec{\kappa}), \tag{2.17c}$$

$$x_4 = \vec{\hat{k}}\cdot\left(\vec{\tau}\times\vec{\xi}\right), \tag{2.17d}$$

$$x_5 = \vec{\rho}\cdot\vec{\tau}, \tag{2.17e}$$

$$x_6 = \vec{\rho}\cdot\vec{\kappa}, \tag{2.17f}$$

$$x_7 = \vec{\rho}\cdot\vec{\xi}, \tag{2.17g}$$

$$x_8 = \vec{\tau}\cdot\vec{\xi}, \tag{2.17h}$$

$$x_9 = \vec{\kappa}\cdot\vec{\xi}, \tag{2.17i}$$

$$x_{10} = \vec{\rho}\cdot\vec{\rho}, \tag{2.17j}$$

$$x_{11} = \vec{\kappa}\cdot\vec{\kappa}, \tag{2.17k}$$

in which $\vec{\tau} = \frac{\partial\vec{\rho}}{\partial s}$, $\vec{\kappa} = \frac{\partial\vec{\tau}}{\partial s}$, $\vec{\xi} = \frac{\partial\vec{\kappa}}{\partial s}$. Note that use is made of the orthonormality property of the Frenet frame in order to simplify the equations of motion.

2.3 Constraint Dynamics

Deriving the equations of motion using the state $q(t) = \begin{bmatrix}\theta(t), & s(t), & w(t), & \psi(t)\end{bmatrix}^\top$ results in a model with no interaction between the plates and the ball, such as 2.13. In order to have interaction, Lagrangian multipliers being a representative of the constraint forces in the system are introduced in this section.

The following two assumptions are made:

1. The ball is in point contact with each of the plates for all times.
2. The ball rolls without slipping on the surface of the plates for all times.

A desirable motion of the BR is one for which both of the above listed assumptions are satisfied. When a motion is found, in simulations, it can be checked whether these two assumptions are valid considering the associated Lagrangian multipliers.

Assumption 1 imposes a constraint on position level

$$w(t) = 0 \quad \forall\, t$$

or on velocity level

$$\dot{w}(t) = 0 \quad \forall\, t. \tag{2.18}$$

The no slip assumption, assumption 2, forces that the speed in the center of mass of the ball is equal to the tangential velocity of the ball at the effective radius R, i.e.

$$\dot{s}(t) + R\dot{\psi}(t) = 0 \quad \forall\, t. \tag{2.19}$$

Both constraint equations 2.18 and 2.19 are integrable with respect to time. Therefore, the holonomic constraints can be written as

$$\begin{bmatrix}\dot{w} \\ \dot{s} + R\dot{\psi}\end{bmatrix} = W\dot{q} = \begin{bmatrix}0 \\ 0\end{bmatrix} \text{ and } W = \begin{bmatrix}0 & 0 & 1 & 0 \\ 0 & 1 & 0 & R\end{bmatrix}. \tag{2.20}$$

The equation of motion can be written in a standard form

$$M(q)\ddot{q} + C(q,\dot{q})\dot{q} + G(q) = Q_{nc} + W^\top \lambda \tag{2.21}$$

where $M(q)$ is the mass matrix, $C(q,\dot{q})$ is the matrix containing Coriolis and centrifugal forces, $G(q)$ a column representing the gravitational forces and λ being the Lagrangian multipliers. The constraint dynamics of the BR in excessive coordinates is given by 2.21, with $M(q)$, $C(q,\dot{q})$, $G(q)$, Q_{nc} and W given in 2.14, 2.15, 2.16, 2.4 and 2.20, respectively.

The Lagrangian multipliers λ_1, λ_2 can be interpreted as constraint forces. Figure 2.3 shows the constraint forces related to the imposed constraints 2.18 and 2.19. The first Lagrangian multiplier λ_1 corresponds with F_n, while the second Lagrangian multiplier λ_2 corresponds with F_s. A desirable motion is one for which the following hold

- The normal force F_n is always positive, i.e.

  $$F_n(t) > 0 \quad \forall\, t,$$

  preventing the ball from departing from the edge of the plates. This condition guarantees that there is always a point contact between the ball and each of the plates.

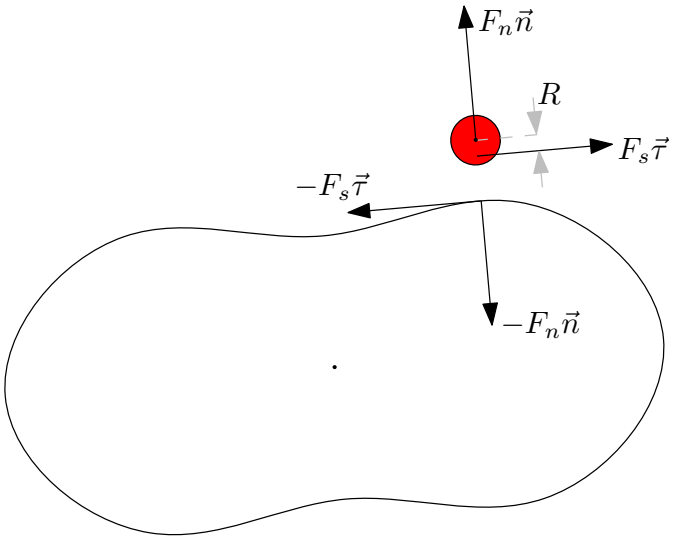

FIGURE 2.3: Constraint forces F_n and F_s represented by λ_1 and λ_2 respectively.

- The friction force F_s should be smaller than the dynamic friction coefficient μ_k times the normal force F_n for the ball to roll without slip, i.e.

$$|F_s| < \mu_k F_n.$$

Explicit equations for the Lagrangian multipliers can be found as follows. First differentiate 2.18 and 2.19 with respect to time to obtain

$$\ddot{w}(t) = 0 \quad \forall\, t, \tag{2.22a}$$

$$\ddot{s}(t) + R\ddot{\psi}(t) = 0 \quad \forall\, t. \tag{2.22b}$$

After, rewriting the equations of motion 2.21 into

$$\ddot{q} = M^{-1}(q)\left(-C(q,\dot{q})\dot{q} - G(q) + Q_{nc} + W^\top \lambda\right), \tag{2.23}$$

explicit equations for $\ddot{w}(t)$ and $\ddot{s}(t) + R\ddot{\psi}(t)$ can be found, which are known to be 0, since 2.22 should hold. This allows for solving λ_1 and λ_2 using for example the software package Maple. The explicit expressions for λ_1 and λ_2 are omitted here, since these are long and complicated. Note that 2.23 is valid since $M(q)$ is positive definite and therefore also invertible.

2.4 Equations of Motion in Generalized Coordinates

The equations of motion can be expressed in generalized coordinates. In comparison with excessive coordinates, generalized coordinates have a lower dimension, which reduces the complexity of further tasks, such as motion planning. However, the model derived in excessive coordinates is still going to be useful to get insight in the constraints forces, which need to be checked for feasible motions.

It is chosen to define the generalized coordinates as $q(t) = \begin{bmatrix}\theta(t) & \varphi(t)\end{bmatrix}^\top$, see Figure 2.4. The equations of motion in excessive coordinates can, in general, be rewritten to equations of motion in generalized coordinates. However, it is easier here to restart with an Euler-Lagrange approach.

Applying a Euler-Lagrange approach yields the equations of motion as

$$\frac{d}{dt}\frac{\partial L}{\partial \dot{q}} - \frac{\partial L}{\partial q} = Q_{nc}^\top,$$

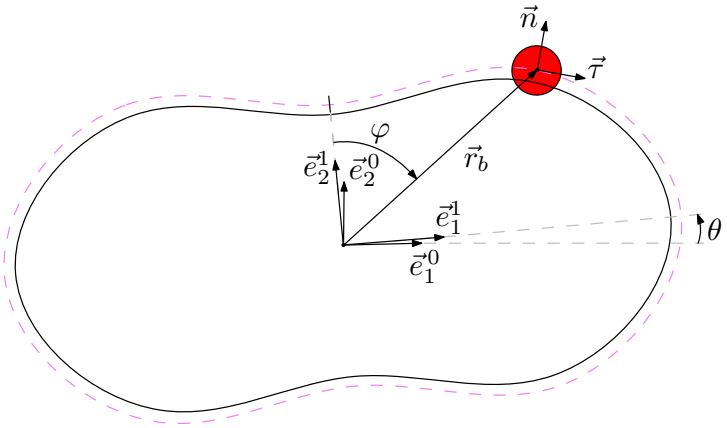

FIGURE 2.4: Generalized coordinates θ and φ.

with, again, L being the Lagrangian of this system defined as the kinetic energy T minus the potential energy V, i.e. $L = T - V$. The row of non-conservative forces Q_{nc} is in this case contains only the torque applied to the center of mass of the plates, i.e.

$$Q_{nc} = \begin{bmatrix} u & 0 \end{bmatrix}.$$

The kinetic energy takes the same expressions for all the components except for the rotational energy of the ball $T_{b,\omega}$. This terms changes because the angular velocity of the ball is now expressed in a different coordinate. The rotational energy of the ball can be expressed as

$$T_{b,\omega} = \frac{1}{2} J_b (\vec{\omega}_b \cdot \vec{\omega}_b), \tag{2.24}$$

with J_b the ball's mass moment of inertia about the $\vec{e}_3^2$ axis and $\vec{\omega}_b = \left(\dot{\theta}(t) + \dot{\varphi}(t)\right) \hat{k}$. The total kinetic energy of the system is

$$T = T_{p,v} + T_{p,\omega} + T_{b,v} + T_{b,\omega}, \tag{2.25}$$

with $T_{p,v}, T_{p,\omega}, T_{b,v}$ and $T_{b,\omega}$ defined in 2.5 to 2.7 and 2.24, respectively. In terms of potential energy, nothing changes.

The Lagrangian of this system is

$$L = T - V, \tag{2.26}$$

with the kinetic energy T given in 2.25 and the potential energy V given in 2.10. Using the software package Maple, the equations of motion can be found en rewritten in the format

$$M(q)\ddot{q} + C(q,\dot{q})\dot{q} + G(q) = Q_{nc}^{\top} = \begin{bmatrix} u \\ 0 \end{bmatrix}, \tag{2.27}$$

with $M(q)$ the mass matrix, $C(q,\dot{q})$ the matrix of Coriolis and centrifugal forces, and $G(q)$ the column of gravitational forces. Specifically, the mass matrix is given by

$$M(q) = \begin{bmatrix} m\vec{\rho}\cdot\vec{\rho} + J_b + J_p & s'\left(m(\vec{\rho}\times\vec{\tau})\cdot\hat{k} - \frac{J_b}{R}\right) \\ s'\left(m(\vec{\rho}\times\vec{\tau})\cdot\hat{k} - \frac{J_b}{R}\right) & (m + \frac{J_b}{R^2})s'^2 \end{bmatrix},$$

the matrix of Coriolis and centrifugal forces is given by

$$C(q,\dot{q} = \begin{bmatrix} ms'\vec{\rho}\cdot\vec{\tau}\dot{\varphi} & m\left(\left((\vec{\rho}\times\vec{\kappa})\cdot\hat{k}s'^2 + s''(\vec{\rho}\times\vec{\tau})\cdot\hat{k}\right)\dot{\varphi} + \dot{\theta}s'\vec{\rho}\cdot\vec{\tau}\right) - \frac{J_b}{R}\dot{\varphi}s'' \\ -m\vec{\rho}\cdot\vec{\tau}s'\dot{\theta} & \dot{\varphi}s''(m + \frac{J_b}{R^2})s' \end{bmatrix},$$

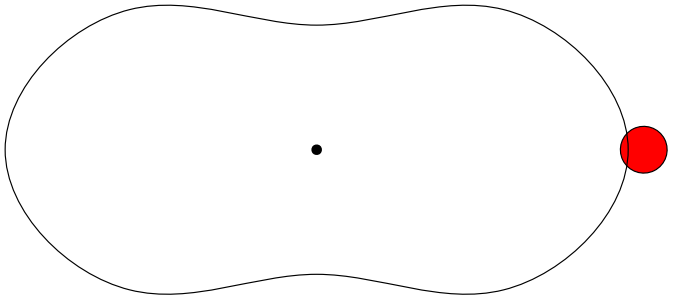

FIGURE 2.5: Illustration of the initial condition used for verification simulations.

TABLE 2.1: Model parameters used for simulations.

Parameters	Description	Value	Unit
d	Distance between the plates	$25 \cdot 10^{-3}$	m
g	Gravitational acceleration	9.81	m s^{-2}
J_b	Moment of inertia of the ball	$5.48 \cdot 10^{-7}$	kg m^2
J_p	Moment of inertia of the plates	$1.581 \cdot 10^{-3}$	kg m^2
m	Mass of the ball	$3.0 \cdot 10^{-3}$	kg
R_b	Radius of the ball	$16.55 \cdot 10^{-3}$	m

and the column of gravitational forces is given by

$$G(q) = m \begin{bmatrix} \vec{g} \cdot (\Pi'(\theta)\vec{\rho}) \\ \vec{g} \cdot (\Pi(\theta)\vec{r}) \end{bmatrix}.$$

The convenience of this Lagrangian modeling approach is that no knowledge about constraint forces is needed for deriving a model with interaction in generalized coordinates.

2.5 Model Verification

The derived models in excessive and generalized coordinates are verified in this section. One of the methods for verification of multiple bodies is to consider the behavior of each body individually, as is done in [2] and [3]. This means that simulations of the corresponding models are performed while the coordinate of one of the two bodies is fixed. Even thought, the models derived here are similar to the models derived in [2] and [3], the verification is performed in order to check the Matlab implementation. In all simulations, the initial condition

$$q_0 = \begin{bmatrix} \theta_0, \varphi_0, \dot{\theta}_0, \dot{\varphi}_0 \end{bmatrix}^\top = \begin{bmatrix} 0, \frac{\pi}{2}, 0, 0 \end{bmatrix}^\top, \tag{2.28}$$

is used, which corresponds to the situation in Figure 2.5. Note that the initial conditions in 2.28 are given in generalized coordinates, but can be rewritten to excessive coordinates. Furthermore, an overview of the model parameters can be found in Table 2.1.

2.5.1 Fixed Ball Verification

When the position of the ball is fixed, the system should behave as a single body in a pendulum like fashion. If the initial conditions are chosen outside an equilibrium and the initial angular velocity of the plates is chosen low enough, then the pendulum will swing around its downward equilibrium $\theta = \frac{-\pi}{2} = \frac{3\pi}{2}$ forever, since there is no damping included in the model.

The results of the model in excessive coordinates are given in Figure 2.6. Note that φ is not an excessive coordinate, but for comparison reasons, it is computed using its relation to other

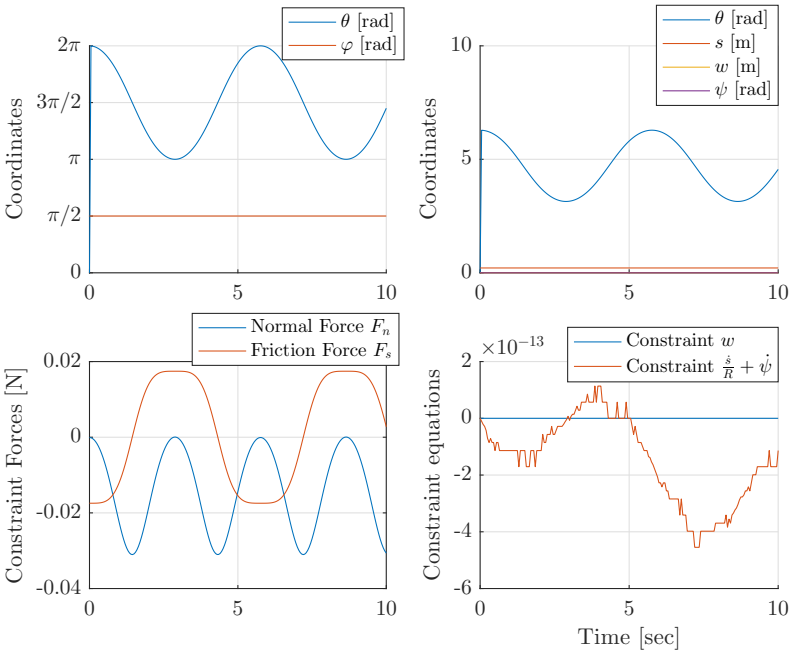

FIGURE 2.6: Simulation results in excessive coordinates with initial conditions 2.28, and a fixed ball position. Left upper plot: Result given in generalized coordinates, but computed from the results in the excessive coordinates. Right upper plot: Results in terms of excessive coordinates. Left bottom plot: Constraint forces over time. Right bottom plot: Constraint equations stay close to 0.

coordinates. The results for the model in generalized coordinates is omitted here, since it behaves exactly the same as the model in excessive coordinates. As expected, the system behaves as a pendulum oscillating around $\theta = \frac{3\pi}{2}$. The coordinate φ corresponding to the position of the ball is fixed. The amplitude of normal force F_n can be checked at the for example the position $\theta = \frac{3\pi}{2}$. It should equal the mass of the ball m times the gravitational acceleration g, i.e. $F_n = m \cdot g = -0.0294$ N, which is true as can be seen in the lower left plot Figure 2.6. Besides that, the sign of F_n is always negative, which is expected, since the ball should lose contact with the plates. Furthermore, the constraint equations are satisfied since these are zero, and behave in a stable fashion since they stay close zero. It this was not the case, then concept of Baumgarte stabilization [7] could be applied.

2.5.2 Fixed Plates Verification

When the position of the plates is fixed, the ball should roll over the edge of the plates. Since there is no damping, the ball should keep rolling for ever. If the initial velocity of the ball is chosen low enough, then the ball will roll from side to side over the plates.

The results for the model in excessive coordinates is given in Figure 2.7. Since the model in generalized coordinates show exactly the same behavior, the results are omitted here. As expected, the coordinate concerning the plates is fixed, i.e. $\theta = 0$, and the ball rolls over the plates from side to side, which indeed corresponds to $\varphi \in [\frac{\pi}{2}, \frac{3\pi}{2}]$ in the left upper plot. The right upper plot shows the results in excessive coordinates. Here is can be seen that the response in ψ and s has the same periodic behavior as the response in φ, which is expected. Furthermore, w and θ stay zero as is supposed to. The constraint forces show expected behavior in the left bottom plot. The normal force F_n should indeed be zero at the start of the simulation, i.e. the situation depicted in Figure 2.5 and at the positions where $\varphi = \frac{3\pi}{2}$. Furthermore, it is intuitive that F_n is positive at $\varphi = \pi$, since the ball is pressed against the frame here. It is also expected

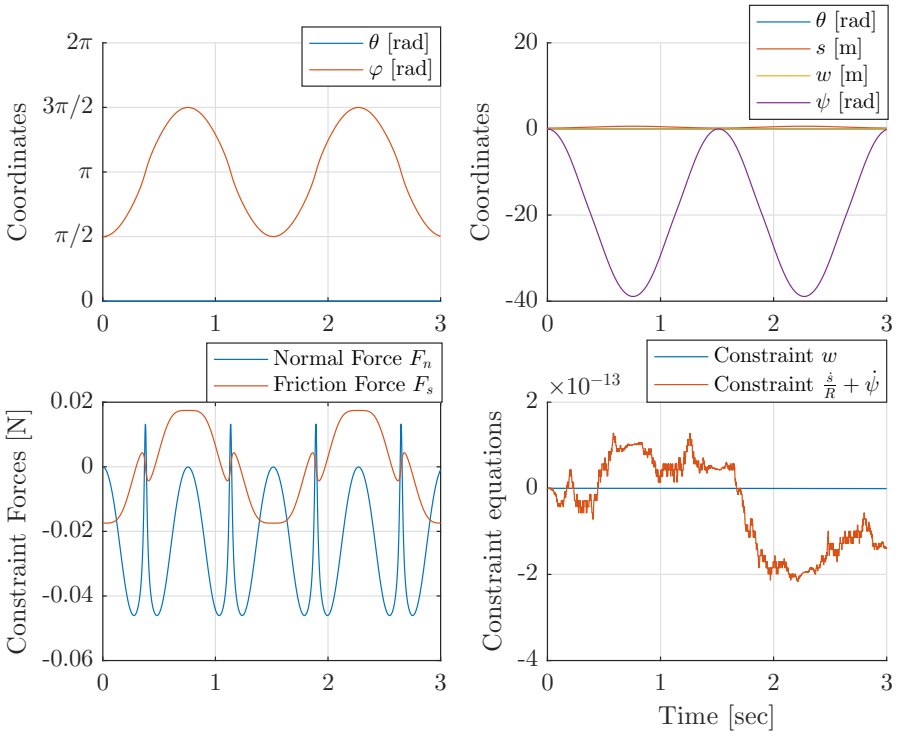

FIGURE 2.7: Simulation results in excessive coordinates with initial conditions 2.28, and a fixed plates position. Left upper plot: Result given in generalized coordinates, but computed from the results in the excessive coordinates. Right upper plot: Results in terms of excessive coordinates. Left bottom plot: Constraint forces over time. Right bottom plot: Constraint equations stay close to 0.

that F_n has mostly a negative sign, meaning that the ball will depart from the plates. The bottom right plot shows that the constraint equations are satisfied since they stay close to zero.

The simulation results in Figure 2.6 and Figure 2.7 show expected behavior. Therefore, it is assumed that both models are accurate.

2.6 Summary

In this chapter, after introducing a more convenient coordinate set, the model of the BR is derived for both excessive and generalized coordinates using a Lagrange approach. The model in generalized coordinates has a lower state dimension and will therefore further be used for motion planning and feedback stabilization. The model in excessive coordinates gives insight in the constraint forces. This model will be utilized to see whether the planned motion satisfies the constraints and thus results in a feasible motion. Both models are validated by means of numerical simulations.

Chapter 3

Motion Planning

In this chapter, the steps taken in planning motions for the BR are discussed. First of all, using phase portraits, the desired motion is described. After that, a virtual holonomic constraint relations is introduced. Next, conditions of feasible motions are given. Then, the actual motion is planned. At the end, a control input providing invariance is derived. Throughout this chapter, the model in generalized coordinates is used, since this model has a lower state dimension and, therefore, reduces the complexity.

3.1 Virtual Holonomic Constraints

A virtual holonomic constraint (VHC) is a virtual constraint imposed on position level, hence the name. Such a constraints relates coordinates to each other and can be made invariant by proper control input. In case of the BR, the ball should be manipulated by the plates in such a way that the task of continuous rolling for the ball is performed. By introducing such a constraint, the dynamics can be reduced in terms of degrees of freedom (DOF), which allows for a constructive procedure for finding feasible trajectories.

For convenience, the dynamics of the system in generalized coordinates are recalled here,

$$M(q)\ddot{q} + C(q,\dot{q})\dot{q} + G(q) = \begin{bmatrix} u \\ 0 \end{bmatrix}, \tag{3.1}$$

with $q = \begin{bmatrix} \theta & \varphi \end{bmatrix}^\top$. It is clear to see that 3.1 has 2 DOF, namely θ and φ, corresponding to the orientation of the plates and the position of the ball respectively. By introducing a VHC of the form $\theta = \Theta(\varphi)$, the DOF can be reduced by one, which leaves only φ as a DOF. The VHC imposes the following relations:

$$\theta = \Theta(\varphi), \tag{3.2a}$$
$$\dot{\theta} = \Theta'(\varphi)\dot{\varphi} \tag{3.2b}$$
$$\ddot{\theta} = \Theta''(\varphi)\dot{\varphi}^2 + \Theta(\varphi)'\ddot{\varphi}, \tag{3.2c}$$

with $\Theta(\varphi)' = \frac{\partial \Theta(\varphi)}{\partial \varphi}$ and $\Theta(\varphi)'' = \frac{\partial^2 \Theta(\varphi)}{\partial \varphi^2}$.

Substituting the relations of 3.2 into 3.1 results in the following reduced dynamics

$$M(\hat{q})\ddot{\hat{q}} + C(\hat{q},\dot{\hat{q}})\dot{q} + G(\hat{q}) = \begin{bmatrix} u \\ 0 \end{bmatrix}. \tag{3.3}$$

These dynamics have only 1 DOF, namely φ, and are associate with the state column (and its time-derivatives) given by

$$\hat{q} = \begin{bmatrix} \Theta(\varphi) \\ \varphi \end{bmatrix}, \quad \dot{\hat{q}} = \begin{bmatrix} \Theta'(\varphi)\dot{\varphi} \\ \dot{\varphi} \end{bmatrix} \text{ and } \ddot{\hat{q}} = \begin{bmatrix} \Theta''(\varphi)\dot{\varphi}^2 + \Theta'(\varphi)\ddot{\varphi} \\ \ddot{\varphi} \end{bmatrix}.$$

If the VHC is made invariant by a certain control input, then the trajectory of the ball is the solution to the zero dynamics of 3.3. The zero dynamics are given by the second equation of 3.3. This is a second order differential equation, which can always be written in the form

$$\alpha(\varphi)\ddot{\varphi} + \beta(\varphi)\dot{\varphi}^2 + \gamma(\varphi) = 0, \tag{3.4}$$

with, specifically for the BR,

$$\alpha(\varphi) = m\left(\left((\vec{\rho}\times\vec{\tau})\cdot\hat{k} - \frac{J_b}{mR}\right)\Theta(\varphi)' + \left(1 + \frac{J_b}{mR^2}\right)s'\right), \tag{3.5a}$$

$$\beta(\varphi) = m\left(\left((\vec{\rho}\times\vec{\tau})\cdot\hat{k} - \frac{J_b}{mR}\right)\Theta(\varphi)'' - \vec{\tau}\cdot\vec{\rho}\,\Theta(\varphi)'^2 + \left(1 + \frac{J_b}{mR^2}\right)s''\right), \tag{3.5b}$$

$$\gamma(\varphi) = mg\begin{bmatrix}\sin(\varphi) & \cos(\varphi)\end{bmatrix}\vec{\tau}. \tag{3.5c}$$

The zero dynamics depend on the choice of the VHC, since $\Theta(\varphi), \Theta'(\varphi)$ and $\Theta''(\varphi)$ are present in $\alpha(\varphi), \beta(\varphi)$ and $\gamma(\varphi)$, 3.5. The solution to the zero dynamics starting from an initial condition $[\varphi_0, \dot{\varphi}_0]$ represents the trajectory of the ball. This observation allows for shaping the motion by analyzing the zero dynamics 3.4.

The VHC should be chosen such that the a solution for the zero dynamics exists and is unique. The zero dynamics, 3.4, can be rewritten to

$$\ddot{\varphi} = \frac{1}{\alpha(\varphi)}\left(-\beta(\varphi)\dot{\varphi}^2 - \gamma(\varphi)\right), \tag{3.6}$$

An unique solution to 3.4 exists if

$$\begin{aligned} \alpha(\varphi) &\neq 0 \quad \forall \quad \varphi \in [0, 2\pi), \\ \beta(\varphi) &< \infty \quad \forall \quad \varphi \in [0, 2\pi), \\ \gamma(\varphi) &< \infty \quad \forall \quad \varphi \in [0, 2\pi), \end{aligned}$$

with $\alpha(\varphi), \beta(\varphi)$ and $\gamma(\varphi)$ in 3.5. Note that since each component in $\alpha(\varphi), \beta\varphi$ and $\gamma(\varphi)$ is periodic, the interval $\varphi \in [0, 2\pi)$ is used here rather than $\varphi \in \mathbb{R}$. The condition on $\alpha(\varphi)$ implies that

$$\Theta(\varphi)' \neq \frac{\left(1 + \frac{J_b}{mR^2}\right)s'}{\left((\vec{\rho}\times\vec{\tau})\cdot\hat{k} - \frac{J_b}{mR}\right)} \,\forall\, \varphi \in [0, 2\pi). \tag{3.7}$$

The condition on $\beta(\varphi)$ implies that the VHC function $\Theta(\varphi)$ is twice differentiable with respect to φ. The third condition, i.e. the condition on γ, is always satisfied due to the components in $\gamma(\varphi)$.

It is worth to notice that the zero dynamics have an explicit integral of motion. This integral of motion preserves it's value along solution of the zero dynamics providing that the initial conditions are chosen appropriately. Existence of the conserved quantity implies that the zero dynamics have no asymptotically stable solutions [8].

After a feasible trajectory is found, the control input imposing this constraint can be found by the first equation of 3.3, which can be written as

$$u = M_1(\hat{q})\ddot{\hat{q}} + C_1(\hat{q}, \dot{\hat{q}})\dot{\hat{q}} + G_1(\hat{q}),$$

with X_i being the i-th row of the matrix X. Writing out the state $\hat{q}$ gives

$$u = M_1(\hat{q}) \begin{bmatrix} \Theta(\varphi)''\dot{\varphi}^2 + \Theta(\varphi)'\ddot{\varphi} \\ \ddot{\varphi} \end{bmatrix} + C_1(\hat{q}, (\dot{\hat{q}})) \begin{bmatrix} \Theta(\varphi)'\dot{\varphi} \\ \dot{\varphi} \end{bmatrix} + G_1(\hat{q}),$$

here, $\ddot{\varphi}$ is given in 3.6, which results in

$$\begin{aligned} u =& M_1(\hat{q}) \begin{bmatrix} \Theta(\varphi)''\dot{\varphi}^2 + \Theta(\varphi)' \frac{1}{\alpha(\varphi)} \left(-\beta(\varphi)\dot{\varphi}^2 - \gamma(\varphi)\right) \\ \frac{1}{\alpha(\varphi)} \left(-\beta(\varphi)\dot{\varphi}^2 - \gamma(\varphi)\right) \end{bmatrix} \\ &+ C_1(\hat{q}, (\dot{\hat{q}})) \begin{bmatrix} \Theta(\varphi)'\dot{\varphi} \\ \dot{\varphi} \end{bmatrix} + G_1(\hat{q}). \end{aligned}$$

In general, the control input imposing the VHC 3.2 can be written as

$$u = \frac{\left[L^{-1}\left(N + M^{-1}CL\begin{pmatrix} 0 \\ \dot{\varphi} \end{pmatrix} + M^{-1}G\right)\right]_1}{[L^{-1}M^{-1}]_{1,1}}, \tag{3.8}$$

with $X_{i,j}$ corresponding to the (i,j)-th element of the matrix X and,

$$L := L(\varphi = \begin{bmatrix} 1 & \Theta'(\varphi) \\ 0 & 1 \end{bmatrix}, \tag{3.9a}$$

$$N := N(\varphi, \dot{\varphi} = \begin{bmatrix} \Theta''(\varphi)\dot{\varphi}^2 \\ 0 \end{bmatrix}, \tag{3.9b}$$

$$M := M(\Theta, \varphi), \tag{3.9c}$$

$$C := C(\Theta, \varphi, \Theta'\dot{\varphi}, \dot{\varphi}), \tag{3.9d}$$

$$G := G(\Theta, \varphi). \tag{3.9e}$$

However, after imposing the VHC, the dynamics will always be unstable, which calls for a stabilizing control law. Designing the stabilizing feedback law will be the topic of the next chapter.

3.2 Desired Motion

The task of the BR is to perform continuous one-directional rollings of the ball on the edge of the plates. This periodic task can be categorized as a periodic motion of the second kind. A periodic motion of the first kind is one which repeats itself after the T seconds, with T the period time, i.e.

$$\varphi(t + kT) = \varphi,\ \dot{\varphi}(t + kT) = \dot{\varphi} \text{ and } k \in \mathbb{Z}.$$

In this case, a period motion of the second kind is searched for. This is represented by the position of the ball always increasing/decreasing and the velocity being periodic, i.e.

$$\varphi(t + kT) = \varphi + 2\pi k,\ \dot{\varphi}(t + kT) = \dot{\varphi} \text{ and } k \in \mathbb{Z}.$$

Note that since the position of the ball always increases/decreases, the (angular) velocity of the ball should always be positive/negative. The difference between these two kinds of periodic motions can be pointed out in the phase portrait, see Figure 3.1. The left figure shows a center around an equilibrium, while the right figure shows a periodic motion, repeating itself over the φ axis. In the phase portrait, these kinds of periodic motions are separated by the so-called separatrix lines, red lines in Figure 3.1.

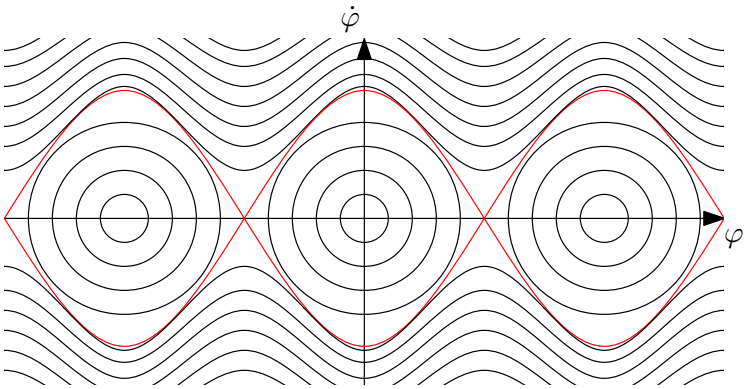

FIGURE 3.1: A periodic motion of the first kind corresponds to a center around an equilibrium point. The velocity of a periodic motion of the second kind does not change sign. These kinds of periodic motions are separated by the separatrix lines (red).

The phase portrait of the zero dynamics, 3.4, can be studied as follows. At the equilibria, the velocity and acceleration are zero, i.e. $\dot{\varphi}_{eq} = \ddot{\varphi}_{eq} = 0$ hence the equilibria can be found by

$$\begin{aligned} \alpha(\varphi_{eq})\ddot{\varphi}_{eq} + \beta(\varphi_{eq})\dot{\varphi}_{eq}^2 + \gamma(\varphi_{eq}) &= 0 \\ \gamma(\varphi_{eq}) &= 0 \end{aligned}$$

Furthermore, the nature of the equilibria can be studies by considering the linearization of the zero dynamics around these equilibria. This leads to

$$\ddot{z} + wz = 0, \text{ with } w = \frac{[\partial]}{\partial\varphi}\frac{\gamma(\varphi)}{\alpha(\varphi)}\bigg|_{\gamma(\varphi_{eq})=0} = \frac{-\gamma'(\varphi(\gamma_{eq}))}{\alpha(\varphi_{eq})}.$$

Depending on the sign of w, the linearized system has either a center of a saddle point. For a positive w , the equilibrium is a center, while for a negative w , the equilibrium is classified as a saddle point, [5].

Having this information, the separatrix lines can be found using the fact that these go through the saddle points. Starting close to the saddle points, the separatrix lines can be found numerically by forward integration of the zero dynamics. The separatrix lines give insight in which initial condition $(\varphi_0, \dot{\varphi}_0)$ can be chosen in order to have a periodic motion of the second kind as the solution of the zero dynamics, 3.4.

An aim for the desired trajectory of the ball is to have a low angular speed $\dot{\varphi}$. This is beneficial for practical implementation, since the position of the ball is being measured by means of a camera. A lower angular speed will result in a more accurate measurement.

3.3 Trajectory for the Butterfly Robot

In the previous sections, the reduced dynamics are found using a VHC. Furthermore, the desired motion is introduced. In this section, the design of the trajectory is described.

As aforementioned, the desired trajectory of the ball should satisfy the zero dynamics. This fact will be used to find a desired trajectory. The procedure used here is as follows:

1. Define a class of VHC functions, for which $\Theta(\varphi)$ is twice differentiable. This class can be based on intuition about and experiences with the system and task.

2. Find the potential parameters by checking condition 3.7 numerically for a grid of parameters. This step reduced the space of parameters which can be selected.

3. Draw the phase portrait of the zero dynamics for various parameters. Search for periodic motions of the second kind for constraints functions in this class.
4. Select suitable parameters. This step defined the VHC function.
5. If no suitable virtual holonomic constraint can be found inside the class, start over with defining another class of VHC functions.

In [5], the following class of virtual holonomic constraints in introduced

$$\Theta(\varphi) := \varphi + \arctan \frac{a \sin(2\varphi - \pi)[\Pi(\varphi)\vec{\tau}]_1 - [\Pi(\varphi)\vec{\tau}]_2}{a \sin(2\varphi - \pi)[\Pi(\varphi)\vec{\tau}]_2 + [\Pi(\varphi)\vec{\tau}]_1}, \tag{3.10}$$

with the parameter

$$a = -0.03. \tag{3.11}$$

Based on the constraint relation in 3.10, the following class of VHCs is introduced here:

$$\theta(\varphi) = \varphi + a \sin(2\varphi) + b \sin(4\varphi), \tag{3.12}$$

which, after choosing suitable parameters $a, b \in \mathbb{R}$, shows similar behavior. Condition 3.7 can be checked numerically using a grid of a and b. The results are shown in Figure 3.2. The filled black dots represent the parameters a and b which satisfy 3.7. Using the results in Figure 3.2 and drawing the phase portrait for various parameter values a and b, it is found that suitable parameters for the class 3.12 are

$$a = 0.585 \text{ and } b = 0.105. \tag{3.13}$$

The resulted phase portrait is given in Figure 3.3. The desired trajectory is the red colored curve in this figure. The associated initial conditions are

$$\varphi_0 = 0 \text{ [rad] and } \dot{\varphi}_0 = 1.9 \text{ [rad/s]}. \tag{3.14}$$

Simulations should show whether the ball stays on the plates throughout the complete motion using this designed trajectory. The model in excessive coordinates, 2.21, should be used for these simulations, since this model gives insight in the constraint forces.

In [5], the VHC function 3.10 with parameter 3.11 and the initial conditions $[\varphi_0, \dot{\varphi}_0] = [0, 0.975]$ were chosen. This resulted in the maximum angular speed $\varphi_{\max} = 1.9$ [rad/sec] and a period time $T = 4.6$ sec. In the case of 3.12 with parameters 3.13 and initial conditions 3.14, the same maximum angular speed $\varphi_{\max} = 1.9$ [rad/sec] is found, as can be seen in the phase portrait Figure 3.3. The period time in this case is 6.6 sec.

The conclusion is that both trajectories have the same maximum angular speed $\varphi_{\max}$, but the newly designed trajectory has a longer period time. This implies that in average the angular speed is lower, since in both cases the ball travels the same distance during one complete rotation of the plates.

From the phase portrait, it can be seen that starting in a different initial condition results in a significantly different trajectory for the ball. This can either be a periodic motions of the first kind or a periodic motion of the second kind. Due to perturbations on the BR in an actual experiment, the trajectory of the ball can be different than designed. Therefore, a feedback controller is designed in the next chapter.

3.4 summary

This chapter presented an approach for motion planning for underactuated systems. After imposing a class of virtual holonomic constraint between the degrees of freedom of the system,

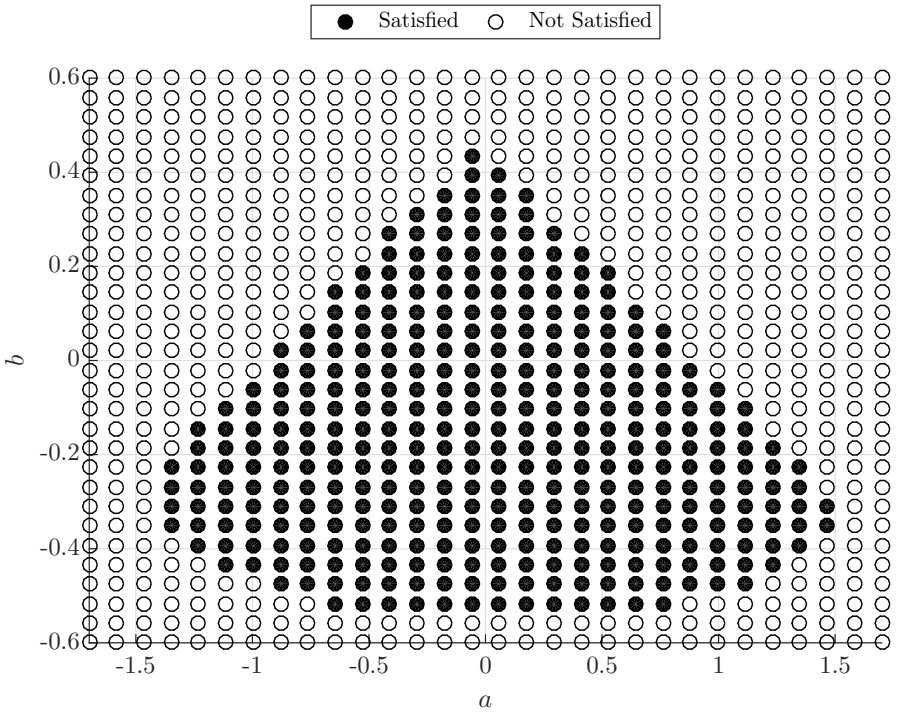

FIGURE 3.2: Condition 3.7 checked numerically for 3.12 using a grid for a and b. The black filled dots represent values for which 3.7 is satisfied, while the parameters corresponding to the transparent dots are in conflict with 3.7.

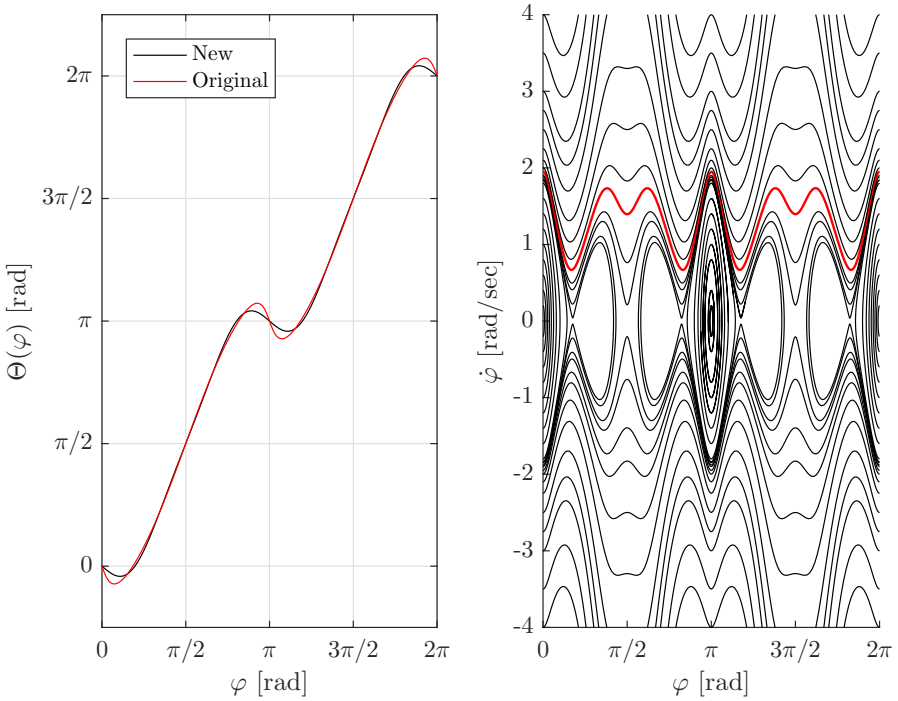

FIGURE 3.3: Left: The virtual holonomic constraint which was proposed in [5] with $a = -0.03$ (labeled as Original) and the newly found virtual holonomic constraint 3.12 with parameters 3.13 (labeled as New). Right: Phase portrait of the zero dynamics 3.4, with the constraint in 3.12 and parameters 3.13. The red line represent the desired trajectory, which starts at the initial conditions $[\varphi_0, \quad \dot{\varphi}_0] = [0, \quad 1.9]$

.

the dynamics can be written in only one DOF, namely the coordinate representing the position of the ball. The desired trajectory of the ball can be shaped by analyzing the phase portrait of the reduced zero dynamics. However, the zero dynamics appear to be unstable and need to be stabilized by means of feedback stabilization.

Chapter 4

Feedback stabilization

The previous chapter described how a desirable periodic motion for the BR is found. This periodic motion is unstable and needs to be stabilized. The design of the stabilizing control law is the topic of this chapter. This chapter is organized as follows. First the notion of orbital stabilization is introduced. Linearization of a system obtained via a particular coordinate transformation results in a periodic Linear Time Varying (LTV) system. This periodic LTV system can be stabilized by linear control techniques. Stability of the origin of this LTV system is equivalent to orbital stability in the vicinity of the periodic motion. At the end of this chapter, a stability analysis is given.

4.1 Orbital Stabilization

Orbital stability is the notion used to classify stability of a periodic motion, as is the case for the BR. Orbital stabilization is the task to find a stabilizing feedback controller renders the nonlinear closed loop system stable around the periodic motion. Stabilizing a periodic motion requires different tools than classical reference tracking control. In concept, the error in classical reference tracking control is evaluated as the difference between the current position and the desired position in time. A drawback of this concept is that the a tracking error is present even when the robot acts delayed or advanced in time on the designed path. This error is not relevant. A more intuitive way of evaluating mismatch from the orbit is to define the error as the distance from a current state of the BR to the orbit of the designed trajectory. This definition will not produce an additional control action when the BR is acting arbitrary shifted in time on the periodic motion.

Stabilization of a given periodic motion requires a change of coordinates such that the dynamics of the BR can be written transverse to the motion's orbit. The next subsection gives a choice of transverse coordinates, which can be used to generate appropriate error signals for the BR. After that, the dynamics of the BR in the vicinity of the desired orbit are derived analytically.

4.1.1 Transverse Coordinates

For the designed periodic motion, 3.12, all the state components are known. The position $\varphi^\star(t)$ and velocity $\dot{\varphi}^\star(t)$ of the ball are found from the solution to the zero dynamics, 3.4, while the orientation $\theta^\star(t) = \Theta(\varphi^\star(t))$ and velocity $\dot{\theta}^\star(t) = \Theta'(\varphi^\star(t))\dot{\varphi}^\star(t)$ of the plates are found from the VHC relations in 3.2. The desired periodic motion can be denoted as

$$q^\star(t) = [\theta^\star(t), \varphi^\star(t)] \text{ and } \dot{q}^\star = \left[\dot{\theta}^\star(t), \dot{\varphi}^\star(t)\right],$$

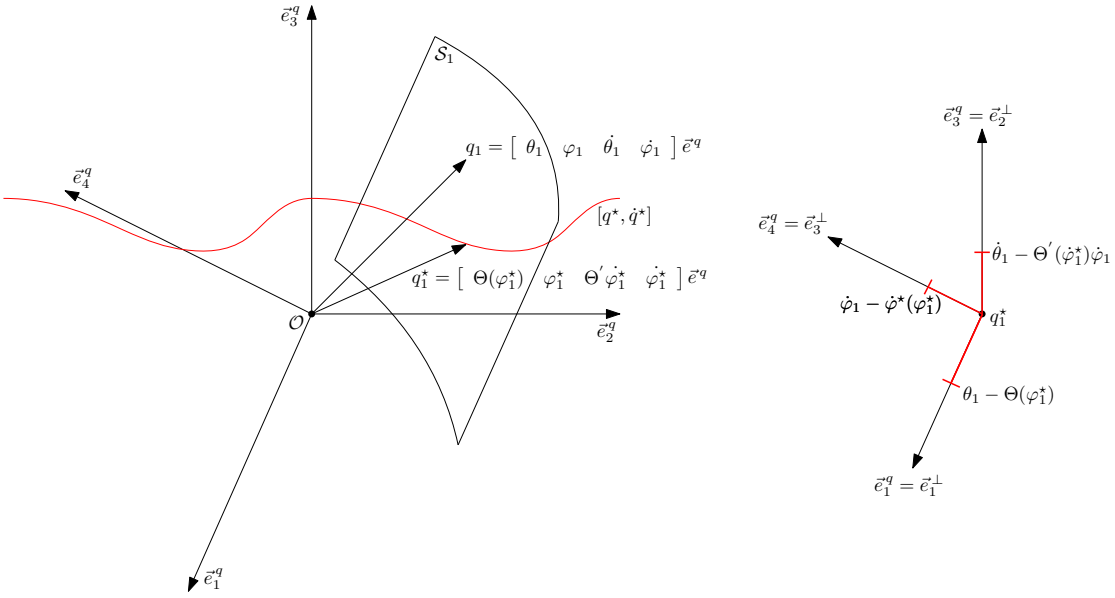

FIGURE 4.1: Left: Moving Poincaré sections $\mathcal{S}_i$ for the desired periodic motion $q^\star$. Right: Transverse coordinates and basis vectors of $\mathcal{S}$ coinciding with a set of the basis vectors of $\vec{e}^q$.

with $q^\star(t) = q^\star(t+T)$ and $\dot{q}^\star = \dot{q}^\star(t+T)$ where T is the period time. Since $\varphi(t)$ monotonically increases within the period, the periodic motion can be parametrized as a function of $\varphi(t)$ instead of time t, i.e.

$$q^\star(t) = \Phi(\varphi^\star(t)) \text{ and } \dot{q}^\star(t) = \frac{\partial \Phi(\varphi^\star(t))}{\partial \varphi^\star(t)} \dot{\varphi}^\star(t), \quad \varphi^\star(t) \in \mathbb{R} \text{ and } t \in [0, T).$$

The concept in transverse dynamics is to introduce a new set coordinates such that the state can be decomposed into:

1. A scalar coordinate representing the position along the the periodic motion.
2. The other coordinates representing the dynamics transverse to the periodic motion, also called transverse coordinates.

It can be noted that the dimension of the transverse dynamics is one less than the original dynamics. These coordinates are called transverse because they vanish when the actual trajectory coincides with the desired trajectory. Therefore, stabilization of the transverse dynamics is equivalent to orbital stabilization of the periodic motion. Another observation is that since $[\dot{q}^\star, \ddot{q}^\star] \neq 0 \, \forall \, t \in [0, T)$ hold, the system can not be in an equilibrium at any moment during the complete motion.

In this case, the coordinate φ is monotonically increasing and can therefore be used to represent the position along the periodic motion. Since the motion is periodic, this results in a periodic $\dot{\varphi}$, θ and $\dot{\theta}$. This allows to define the moving Poincaré sections as

$$\mathcal{S}_i := \{q \in \mathbb{R}^4 \,|\, \varphi_i = \varphi_i^\star\} \quad \forall \quad \varphi \in [0, 2\pi), \tag{4.1}$$

with i denoting the index of the section. Each Poincaré section is nothing more than a three dimensional subspace of the complete state space $\mathbb{R}^4$ obtained by fixing the axis corresponding to φ, see Figure 4.1. An obvious choice for the basis vectors is

$$\vec{e}^{\,\perp} = \begin{bmatrix} 1 & 0 & 0 & 0 \\ 0 & 0 & 1 & 0 \\ 0 & 0 & 0 & 1 \end{bmatrix} \vec{e}^q, \tag{4.2}$$

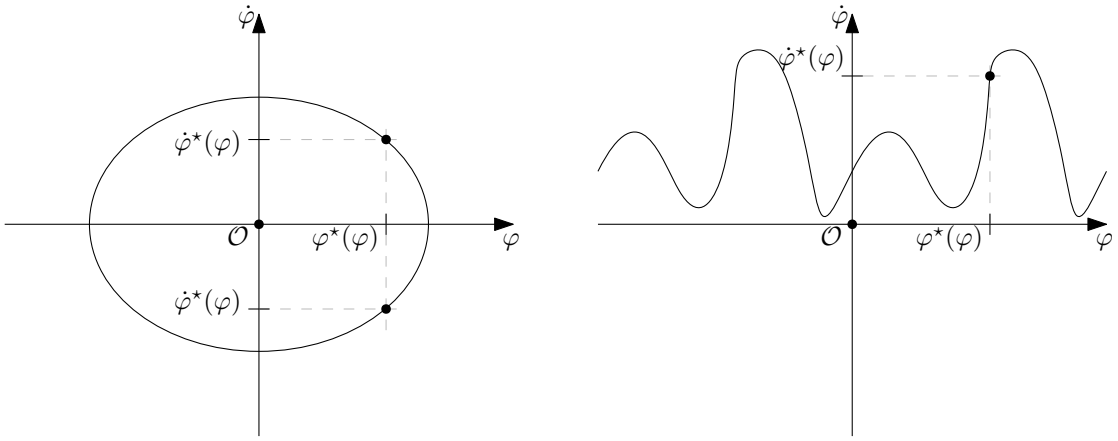

FIGURE 4.2: Illustrative example showing the uniqueness of the third transverse coordinates in relation with periodic motion of the first kind (left) and periodic motions of the second kind (right).

with the transverse coordinates

$$x_\perp = \begin{bmatrix} \theta - \Theta(\varphi^\star) \\ \dot{\theta} - \frac{\partial \Theta(\varphi^\star)}{\partial \varphi}\dot{\varphi} \\ \dot{\varphi} - \dot{\varphi}^\star(\varphi^\star) \end{bmatrix}, \tag{4.3}$$

with $\varphi^\star = \varphi$ and $\dot{\varphi}(\varphi^\star)$ the designed velocity of the ball. Each of the transverse coordinates represents the error on each of the basis vectors $\vec{e}^{\perp}$ and has its origin on the desired periodic motion. Note that this set of transverse coordinates only works for periodic motions of the second kind, i.e. periodic motions where the ball rolls continuously in only one direction. If periodic motion of the first kind are considered, then $\dot{\varphi}^\star$ is not uniquely defined for each φ, see Figure 4.2 for a illustrative example and graphical interpretation in dimension two.

As stated in [5], in general for a system with underactuation degree of 1, the transverse coordinates can be taken as

$$x_\perp = \begin{bmatrix} \theta - \Theta(\varphi^\star) \\ \dot{\theta} - \frac{\partial \Theta(\varphi^\star)}{\partial \varphi}\dot{\varphi}^\star \\ I_0(\varphi, \dot{\varphi}, \varphi_0, \dot{\varphi}_0) \end{bmatrix},$$

with $I_0(\varphi, \dot{\varphi}, \varphi_0, \dot{\varphi}_0)$ being the integral of motion defined as

$$I_0(\varphi, \dot{\varphi}, \varphi_0, \dot{\varphi}_0) = \dot{\varphi}^2 - \exp\left\{-2\int_{\varphi_0}^{\varphi} \frac{\beta(\tau)}{\alpha(\tau)} d\tau\right\}\left(\varphi_0^2 - \int_{\varphi_0}^{\varphi} \exp\left\{2\int_{\varphi_0}^{s} \frac{\beta(\tau)}{\alpha(\tau)} d\tau\right\} \frac{2\gamma(s)}{\alpha(s)} ds\right). \tag{4.4}$$

The integral of motion yields an unique distance to the periodic motion, which makes its useful as a transverse coordinate for periodic motions of the first and second kind. Furthermore, it is possible to derive the transverse dynamics analytically using the integral of motion, which is given in [3] and [9]. However, the integral of motion has a complicated expression, which is unattractive for online computations in simulations/experiments. Therefore, in this case, the transverse coordinates defined in 4.3 are preferred.

A disadvantage of either of the choices for the transverse coordinates is that the third coordinate is found by evaluating the model. More specifically, in the integral of motion 4.4, $\alpha(\varphi), \beta(\varphi)$ and $\gamma(\varphi)$ appear explicitly. In 4.3, the third coordinate contains the term $\dot{\varphi}^\star$, which is calculated in the previous chapter using forward integration of the zero dynamics 3.4. In case the model is inaccurate, $\alpha(\varphi), \beta(\varphi), \gamma(\varphi)$ and $\dot{\varphi}^\star$ can be inaccurate, which could lead to unexpected experimental results. However, no alternative set of transverse coordinates is found yet, which does not need model information for at least one of the transverse coordinates.

In order to analyze in which part of the state-space the transformation from $q \to \begin{bmatrix} x_\perp, & \varphi \end{bmatrix}^\top$ is well-defined, the determinant of the Jacobian of the new state with respect to the old state is considered. In the parts of the state-space where this determinant equals zero, the transformation is not well-defined. This determinant can be worked out as

$$\det\left(\frac{\partial \begin{bmatrix} x_\perp^\top, & \varphi \end{bmatrix}^\top}{\partial q}\right) = \begin{vmatrix} 1 & 0 & 0 & 0 \\ 0 & 0 & 1 & 0 \\ 0 & 0 & 0 & 1 \\ 0 & 1 & 0 & 0 \end{vmatrix} = 1 \,\forall\, q.$$

This shows that the transformation is well-defined for the complete state-space.

4.1.2 Transverse Dynamics

The transverse dynamics describe the state of the system with respect to the desired periodic trajectory. They will have the form

$$\dot{x}_\perp = f_\perp(t, x_\perp). \tag{4.5}$$

The time derivative of the state transverse coordinates $x_\perp$ can be found as follows. Define the first coordinate to be y, i.e.

$$y = \theta - \Theta(\varphi).$$

Then the state q can be written as

$$q = \underbrace{\begin{bmatrix} \theta \\ \varphi \end{bmatrix}}_{\hat{q}} = \begin{bmatrix} y + \Theta(\varphi) \\ \varphi \end{bmatrix},$$

with the time derivatives

$$\begin{aligned} \dot{q} &= \begin{bmatrix} \dot{\theta} \\ \dot{\varphi} \end{bmatrix} = \begin{bmatrix} \dot{y} + \Theta'(\varphi)\dot{\varphi} \\ \dot{\varphi} \end{bmatrix} = L \underbrace{\begin{bmatrix} \dot{y} \\ \dot{\varphi} \end{bmatrix}}_{\dot{\hat{q}}}, \\ \ddot{q} &= \begin{bmatrix} \ddot{\theta} \\ \ddot{\varphi} \end{bmatrix} = \begin{bmatrix} \ddot{y} + \Theta''(\varphi)\dot{\varphi}^2 + \Theta'(\varphi)\ddot{\varphi} \\ \ddot{\varphi} \end{bmatrix} = L \underbrace{\begin{bmatrix} \ddot{y} \\ \ddot{\varphi} \end{bmatrix}}_{\ddot{\hat{q}}} + N, \end{aligned} \tag{4.6}$$

with L and N defined in 3.9a and 3.9b, respectively. Using the invertibility property of L, 4.6 can be rewritten to

$$\ddot{\hat{q}} = L^{-1}\left(\ddot{q} - N\right), \tag{4.7}$$

with $\ddot{q}$ following from 2.27 as

$$\ddot{q} = M(\hat{q})^{-1}\left(Q_{nc} - G(\hat{q}) - C(\hat{q}, \dot{\hat{q}})L\dot{\hat{q}}\right), \tag{4.8}$$

where the mass matrix is positive definite, i.e. $M(\hat{q}) \succ 0$ ensuring that its inverse exists. Substituting 4.8 into 4.7 results in

$$\ddot{\hat{q}} = L^{-1}\left(M(\hat{q})^{-1}\left(Q_{nc} - G(\hat{q}) - C(\hat{q}, \dot{\hat{q}})L\dot{\hat{q}}\right) - N\right)$$

which, for convenience, is rewritten to

$$\ddot{\hat{q}} = \begin{bmatrix} P_1(\hat{q}, \dot{\hat{q}}) \\ P_2(\hat{q}, \dot{\hat{q}}) \end{bmatrix} + \begin{bmatrix} K_1(\hat{q}) \\ K_2(\hat{q}) \end{bmatrix} u,$$

with K_i, P_i, $i = 1, 2$ being scalar functions of $\hat{q}$ and $\dot{\hat{q}}$. Using a partial feedback control law

$$u = K_1^{-1}(\hat{q}) \left(v - P_1(\hat{q}, \dot{\hat{q}}) \right),$$

leaves the linear y dynamics

$$\ddot{y} = v.$$

The φ dynamics become then

$$\ddot{\varphi} = P_2(\hat{q}, \dot{\hat{q}}) + K_2(\hat{q})(K_1^{-1}(\hat{q})(v - P_1(\hat{q}, \dot{\hat{q}}))),$$

which can be written in terms of the zero dynamics as

$$\alpha(\varphi)\ddot{\varphi} + \beta(\varphi)\dot{\varphi}^2 + \gamma(\varphi) = f(\hat{q}, \dot{\hat{q}}),$$

with $\alpha(\varphi), \beta(\varphi)$ and $\gamma(\varphi)$ given in 3.5 and $f(\hat{q}, \dot{\hat{q}})$ being a scalar function arising from the fact that the actual trajectory can deviate from the nominal trajectory. Furthermore, using the Hadamard's Lemma [9], [10], f can be written as a combination of the transverse state components as

$$f(\hat{q}, \dot{\hat{q}}) = f_y y + f_{\dot{y}} \dot{y} + f_v v,$$

with

$$f_y = -ms' \left(\vec{\hat{k}} \cdot (\vec{\rho} \times \vec{\tau}) - \frac{J_b}{mR} \right), \tag{4.9a}$$

$$f_{\dot{y}} = ms' \vec{\tau} \cdot \vec{\rho} (\dot{y} + 2\Theta'(\varphi)\dot{\varphi}), \tag{4.9b}$$

$$f_v = mgs' \mathrm{sinc}\left(\frac{y}{2}\right) \begin{bmatrix} 1, & 0 \end{bmatrix} \cdot (\Pi(y + \Theta(\varphi))\vec{\tau}). \tag{4.9c}$$

Note that the above equations are found using the software package Maple. Having derived all of the above, the transverse dynamics can be given as

$$\dot{x}_\perp = \begin{bmatrix} \dot{y} \\ \ddot{y} \\ \dot{z} \end{bmatrix} = f_\perp(x_\perp, t) \begin{bmatrix} \dot{y} \\ v \\ \frac{1}{\alpha(\varphi)} \left(-\beta(\varphi)(z^2 + \dot{\varphi}^\star z) + \frac{\gamma(\varphi)}{\dot{\varphi}^\star} + f_y y + f_{\dot{y}} \dot{y} + f_v v \right) \end{bmatrix}. \tag{4.10}$$

4.1.3 Transverse Linearization

In order to apply linear control techniques, the transverse dynamics 4.10 are linearized along the desired trajectory. Stabilization of the linearized transverse dynamics guarantees stability of the transverse dynamics close to the periodic orbit, which in turns guarantees stability of the designed periodic motion for the original dynamics in 2.27.

A linear approximation of 4.10 looks like

$$\dot{\xi}(t) = A(t)\xi(t) + B(t)v, \tag{4.11}$$

where the periodic $A(t)$ and $B(t)$ matrices can be found as

$$A(t) = \left. \frac{\partial f_\perp(x_\perp, t)}{\partial x_\perp} \right|_{\varphi=\varphi^\star, \dot{\varphi}=\dot{\varphi}^\star, x_\perp = 0} = \begin{bmatrix} 0 & 1 & 0 \\ 0 & 0 & 0 \\ \frac{1}{\alpha(\varphi^\star)} f_{y^\star} & \frac{1}{\alpha(\varphi^\star)} f_{\dot{y}^\star} & \frac{1}{\alpha(\varphi^\star)} \left(-\beta(\varphi^\star)\dot{\varphi}^\star + \frac{\gamma(\varphi^\star)}{\dot{\varphi}^\star} \right) \end{bmatrix}$$

and

$$B(t) = \left. \frac{\partial f_\perp(x_\perp, t)}{\partial v} \right|_{\varphi=\varphi^\star, \dot{\varphi}=\dot{\varphi}^\star, x_\perp = 0} = \begin{bmatrix} 0 \\ 1 \\ \frac{1}{\alpha(\varphi^\star)} f_{v^\star} \end{bmatrix},$$

with $f_{y^\star}, f_{\dot{y}^\star}$ and $f_{v^\star}$ being 4.9 evaluated on $\varphi = \varphi^\star, \dot{\varphi} = \dot{\varphi}^\star, x_\perp = 0$. The obtained system 4.11 is one in the class of Periodic Linear Time Varying (LTV) system. Note that a recalculation of $A(t)$ and $B(t)$ is needed every time the motion found in Chapter 3 is redesigned.

4.2 Linear Control Techniques

As mentioned before, orbital stabilization of the periodic motion is equivalent to stabilization of the origin of the linearized transverse dynamics. First of all, the question whether a stabilizing feedback exists is answered using the notion of controllability. Next, a method for computing a stabilizing state feedback controller for linear time varying systems is introduced and applied. This method is known as a Linear Quadratic Regulator.

4.2.1 Controllability

A necessary and sufficient condition for a stabilizing controller to exist is the stabilizability property of the pair $(A(t), B(t))$. Stabilizability is implied by controllability, which can be verified by the Controllability Gramian matrix

$$W(0,T) = \int_0^T e^{A(t)t} B(t) B(t)^\top e^{A(t)^\top t} dt$$

being positive definite. This test can be conducted numerically, which results in the following eigenvalues for $W(0,T)$

$$\lambda_1 = 1, \lambda_2 = 1, \lambda_3 = 1,$$

which are all positive. Hence, the pair $(A(t), B(t))$ is controllable, and therefore also stabilizable.

4.2.2 Linear Quadratic Regulator

The linearized transverse dynamics are proven controllable above. A control technique known as Linear Quadratic Regulator (LQR) [9], is the topic of this subsection. The linear quadratic regulator is a state feedback controller which is optimal with respect to a defined quadratic cost function.

This problem can be solved over a finite time horizon, since the system matrix $A(t)$ and the input matrix $B(t)$ are periodic over T. The finite horizon LQR problem reads as follows:

$$\begin{aligned} \min_{v(t), t\in[0,T)} \int_0^T \left(\xi(t)^\top Q \xi(t) + v(t)^\top \Gamma v(t)\right) dt \\ \text{s.t. } \dot{\xi}(t) = A(t)\xi(t) + B(t)v(t), \end{aligned} \tag{4.12}$$

where $Q \succ 0$ is the weighting matrix penalizing error in the state and $\Gamma > 0$ a scalar penalizing control inputs. The optimal solution minimizing 4.12 is

$$v(t) = K(t)\xi(t), \quad K(t) = -\Gamma^{-1} B(t)^\top X(t),$$

with $X(t)$ being the unique periodic positive definite solution (i.e. $X(t) = X(t+T) \succ 0$) to the Periodic Riccati Differential Equation (PRDE)

$$-\dot{X}(t) = A(t)^\top X(t) + X(t)A(t) - X(t)B(t)\Gamma^{-1}(t)B(t)^\top X(t) + Q(t). \tag{4.13}$$

4.2.3 Solution to the Periodic Differential Ricatti Equation

There are multiple approaches available to solve the PDRE. Among them are the one-shot and multi-shot approach, see for example [11]. The approach used here is known as the Convex Optimization approach, which is treated in [6]. An objective function subjected to Linear Matrix Inequality (LMI) constraints is optimized to find the solution to the PDRE defined in 4.13.

Define the Riccati operator as

$$\mathcal{R}(t) = \dot{X}(t) + A(t)^\top X(t) + X(t)A(t) - X(t)B(t)\Gamma^{-1}(t)B(t)^\top X(t) + Q(t). \tag{4.14}$$

According to [6], if one can find a solution $X(t)$ of the Riccati differential inequality

$$\mathcal{R} \geq 0, \forall\, t \geq 0, \tag{4.15}$$

then there exists a solution $X_+(t)$ of the PDRE, where

$$X_+(t) \geq X(t), \forall\, t \geq 0. \tag{4.16}$$

The solution $X_+(t)$ is called the unique maximal T-periodic stabilizing solution. Since 4.16 forces the matrix $X_+(t) - X(t)$ to be semi-positive definite for all time instances, it follows that the eigenvalues of $X_+(t)$ should be greater than or equal to the eigenvalues of $X(t)$, i.e.

$$\lambda(X_+(t)) \geq \lambda(X(t)) \forall\, t.$$

It is well-known that the sum of the Eigenvalues of a matrix is equal to the trace of a matrix, i.e.

$$\sum_{i=1}^{n} \lambda_i(A(t)) = \mathrm{tr}(A(t)).$$

This fact can be used to define the objective function as

$$J(X(t)) = \int_0^T \mathrm{tr}\,(X(t))\, dt \tag{4.17}$$

Finding the solution $X(t)$ which maximizes $J(X(t))$ will end up in the maximal T-periodic stabilizing solution.

Using the Schur Complement, the Riccati inequality 4.15 can be turned into an LMI

$$S(X(t), t) = \begin{bmatrix} \dot{X}(t) + A(t)^\top X(t) + X(t)A(t) + Q(t) & X(t)B(t) \\ B(t)^\top X(t) & \Gamma(t) \end{bmatrix} \succeq 0 \forall\, t. \tag{4.18}$$

Since the problem can be evaluated at each time moment within the period, there is an infinite number of LMIs in the form of 4.18. The solution to this problem can be approximated by a solving the problem over a finite number of N time instances. Furthermore, since the solution $X(t)$ and its time-derivative $\tilde{X}(t)$ are assumed to be T-periodic, it is attractive to approximate them as a truncated Fourier series as

$$\tilde{X}(t) = \sum_{k=-M}^{M} e^{ik\omega t} X_k, \text{ and } \dot{\tilde{X}}(t) = \sum_{k=-M}^{M} ik\omega e^{ik\omega t} X_k,$$

where X_{-k} is the complex conjugate of X_k, $q \in \mathbb{Z}$ is the number of Fourier coefficient matrices and $\omega = \frac{2\pi}{T}$ is the base frequency with T being the period time of the planned motion. The approximation for $S(X(t), t)$, 4.18, is consequently $S(\tilde{X}(t), t)$. Replacing $X(t)$ with $\tilde{X}(t)$ in the

objective function 4.17, results in

$$J(\tilde{X}(t)) = \int_0^T \operatorname{tr}\left(\tilde{X}(t)\right) dt = \int_0^T \operatorname{tr}\left(\sum_{k=-M}^{M} e^{ik\omega t} X_k\right) dt.$$

The integral of each Fourier component with $k \neq 0$ results in 0, since this is an integration over one (or multiple) full period(s). The only component left in the objective function is

$$J(\tilde{X}(t)) = tr(X_0)T$$

which is equivalent to the objective function

$$J(\tilde{X}(t)) = tr(X_0), \tag{4.19}$$

since $T > 0$.

The optimization problem reads then as follows

$$\begin{aligned} \min \quad & -J(\tilde{X}(t)) \\ \text{s.t.} \quad & S_j \geq 0, \quad j = 1, \ldots, N, \end{aligned} \tag{4.20}$$

with the objective function $J(\tilde{X})$ in 4.19. Note that minimizing $-J(\tilde{X}(t))$ is equivalent to maximum $J(\tilde{X}(t))$.

An important theorem in [6] states that

$$||X_+ - \tilde{X}_+||_C \to 0 \quad \text{as} \quad M \to \infty \text{ and } \frac{N}{M^3} \to \infty, \tag{4.21}$$

with $||D||_c = \max_{t\in[0,T)} ||D(t)||$, meaning that the approximated solution converges to the real solution. This shows the ratio between the number of points in time $N \in \mathbb{Z}$ and the number of Fourier components $M \in \mathbb{Z}$. However, in many numerical examples [6], it is shown that this ratio is conservative, i.e. an accurate approximate $\tilde{X}(t)$ of the stabilizing solution $X(t)$ is found by solving 4.20 for N being a significant lower number as stated in 4.21. Furthermore, 4.21 shows that the approximate is not only accurate on the time moments for which 4.20 is solved, but also for the time moments in between, i.e. for all time $t \in [0, T)$.

The optimization problem 4.20 is solved using Matlab for $N = 1000$ and $M = 40$. As a function of φ, the controller gains $k_y, k_{\dot{y}}$, and k_z are given in the upper plot of Figure 4.3. Here it can be observed that these gains are periodic with period $\frac{T}{2}$, which is expected since the shape of the plates of the BR is symmetric. The lower plot of Figure 4.3 shows that the real part of all the eigenvalues of the solution X of the PDRE 4.15 is positive for each φ, which ensures positive definiteness at each time moment. Stability of this controlled system is assessed at the end of this chapter.

The optimization problem 4.20 has a solution for every $Q \succ 0$ and $\Gamma > 0$. Therefore, after a trajectory is found and the periodic $A(t)$ and $B(t)$ matrices are found, a feedback controller can be calculated using the Matlab implementation of 4.20. This reduces the challenge of finding a stabilizing feedback law to running a piece of Matlab code. Note that 4.20 does not have a solution for every N and M.

Another method to design a stabilizing state feedback for the periodic LTV system 4.11 is a Lyapunov approach, presented in Appendix A. However, no stabilizing state feedback is found using this method. Due to time restrictions, this method is not further elaborated.

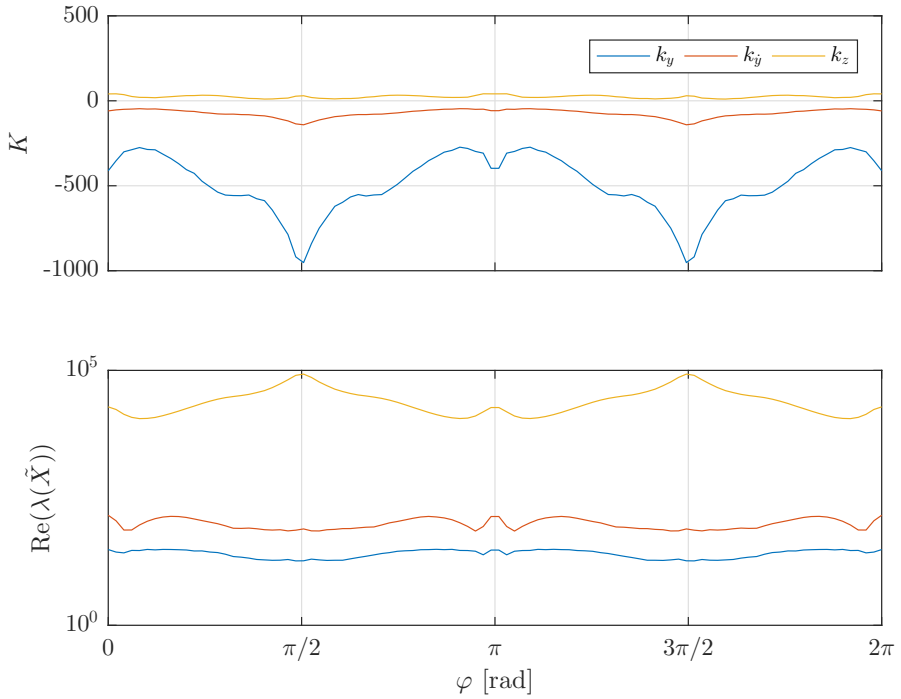

FIGURE 4.3: Upper plot: Control gains as a function of $\varphi \in [0, 2\pi)$. Lower plot: Eigenvalues of $\tilde{X}$ on a logarithmic y-axis showing that X is positive definite for all $\varphi \in [0, 2\pi)$.

4.3 Stability analysis

The closed loop system has the form

$$\dot{\xi}(t) = \underbrace{(A(t) - B(t)K(t))}_{\mathcal{A}(t)}\xi(t), \tag{4.22}$$

with $\mathcal{A}(t+T) = \mathcal{A}(t)$, which is in the class of autonomous periodic linear time-varying systems. For this class of systems, the Floquet Theory is used to assess stability. The Floquet Theory states that the state transition matrix $\Phi(T, 0)$ can written as e^{RT} and that exponential stability of Equation (4.22) is guaranteed if and only if the constant matrix R has all it's eigenvalues located in the open left half-plane, i.e. is Hurwitz, see [12].

First, an expression for the state transition matrix $\Phi(T, 0)$ is found. In general, the solution of Equation (4.22) can be written as

$$\xi(t) = \Phi(t, t_0)\,\xi(t_0), \tag{4.23}$$

starting in $\xi(t_0)$ at t_0. Using $t = t_0$ in Equation (4.23), the following property of the state transition matrix can be derived

$$\Phi(t_0, t_0) = I \,\forall\, t_0. \tag{4.24}$$

To find the state transition matrix, Equation (4.23) can differentiated with respect to time and then set equal to Equation (4.22), which results in

$$\begin{aligned}\dot{\xi}(t) &= \dot{\Phi}(t, t_0)\xi(t_0) \\ &= \mathcal{A}(t)\,\xi(t) \\ &= \mathcal{A}(t)\,\Phi(t, t_0)\,\xi(t_0).\end{aligned}$$

It follows that

$$\dot{\Phi}(t, t_0) = \mathcal{A}(t)\,\Phi(t, t_0),$$

which is an initial value problem. This initial value problem can be solved (numerically) using forward integration with the initial condition given Equation (4.24) for $t_0 = 0$ and $t = T$. Now the constant matrix R can be found using

$$e^{RT} = \Phi(T, 0).$$

In this case, the control gain $K(t)$ is computed using a LQR approach. The state transition matrix is given as

$$\Phi(T, 0) = 10^{-11} \cdot \begin{bmatrix} -0.034 & -0.017 & 0.072 \\ 0.072 & 0.036 & -0.150 \\ -0.207 & -0.104 & 0.431 \end{bmatrix}.$$

It can be observed that all the entries of this matrix tend to go to 0, which implies that the eigenvalues of R must all be located in the open left half-plane. This guarantees both exponential stability for the origin of the linear time-varying system in 4.22, as well as exponential orbital stability in some neighborhood of the desired periodic trajectory for the original nonlinear system in 2.27.

4.4 Summary

This chapter presented an approach to stabilize the periodic motion found in the previous chapter. First of all, a coordinate transformation is applied which allows to write the state of the BR as a scalar representing the position on the orbit, and the other coordinates representing the error transverse to the orbit. These coordinates are called transverse, since they vanish when the BR acts on the desired periodic trajectory. The dynamics are rewritten in transverse coordinates and are linearized in the vicinity of the planned motion. The resulted system is in the class periodic linear time-varying. An LQR approach is used to compute a stabilizing control law. This involves solving a Periodic Differential Riccati Equation, which is performed using a Convex Optimization approach. Another approach to design a stabilizing state feedback controller uses the notion of Periodic Lyapunov functions. However, due to time consideration, the work on the Lyapunov approach is unfinished. Stability of the controlled BR with the controller found using the LQR approach is proven numerically by means of the Floquet Theory. This completes this chapter on feedback stabilization. The next chapter discusses the behavior of the controlled BR.

Chapter 5

Numerical Analysis of the Controlled Butterfly Robot

In Chapter 3, a periodic trajectory is found for the BR, which is stabilized in Chapter 4. This chapter gives the simulation results of the BR with initial conditions starting on the designed trajectory. Furthermore, a region of attraction for the controller BR is found numerically and given. Ideally, the results would be implemented on a real setup in order to investigate the behavior in practice. However, since there is no real setup available, the results are merely based on simulations.

5.1 Starting on the Periodic Motion

In Chapter 3, a periodic motion of the second kind was found. Starting from any initial condition on the periodic motion, the BR should perform the periodic motion in a stable fashion. Furthermore, the conditions on the normal force should be considered, to see whether the ball stays on the edge of the plates, i.e. $F_n > 0 \, \forall \, t$ or whether it departs $F_n < 0$ for some t. In order to get this insight, the model in excessive coordinates 2.21 is considered for these simulations. The results of a 10 seconds simulation for the initial conditions

$$q_0 = \begin{bmatrix} \Theta(\varphi_0), & \varphi_0, & \Theta'(\varphi_0)\varphi^\star(\varphi_0), & \varphi^\star(\varphi_0) \end{bmatrix}^\top, \quad \varphi_0 = 0, \tag{5.1}$$

is shown in Figure 5.1. Here, in the upper left plot, it can be seen that the transverse coordinates stay close to zero, meaning that the BR indeed follows the planned trajectory. They do not go to exactly zero, which is most likely caused by numerical inaccuracies in some of the steps taken in modeling, motion planning and feedback stabilization. In the upper right plot, it can be seen $F_n > 0 \, \forall t \in [0, 10]$, which ensures that the ball does not departs from the frame. The friction force F_s is close to zero. Since the exact value for the dynamic friction coefficient μ_k is unavailable, no conclusions about slip can be drawn. The upper left plot shows that the virtual relation $\theta = \Theta(\varphi)$, defined in 3.2, between the coordinates θ and φ is maintained. Furthermore, the upper right plot shows trajectory on the $(\varphi, \dot{\varphi}$ plane, which matches the designed trajectory in Figure 3.3. It can be concluded that using the trajectory found in Chapter 3 and the feedback controller designed in Chapter 4, the BR performs a periodic motion of the second kind. The next step is to investigate what happens when there is a deviation from the designed trajectory, which is likely to happen in a practical experiment.

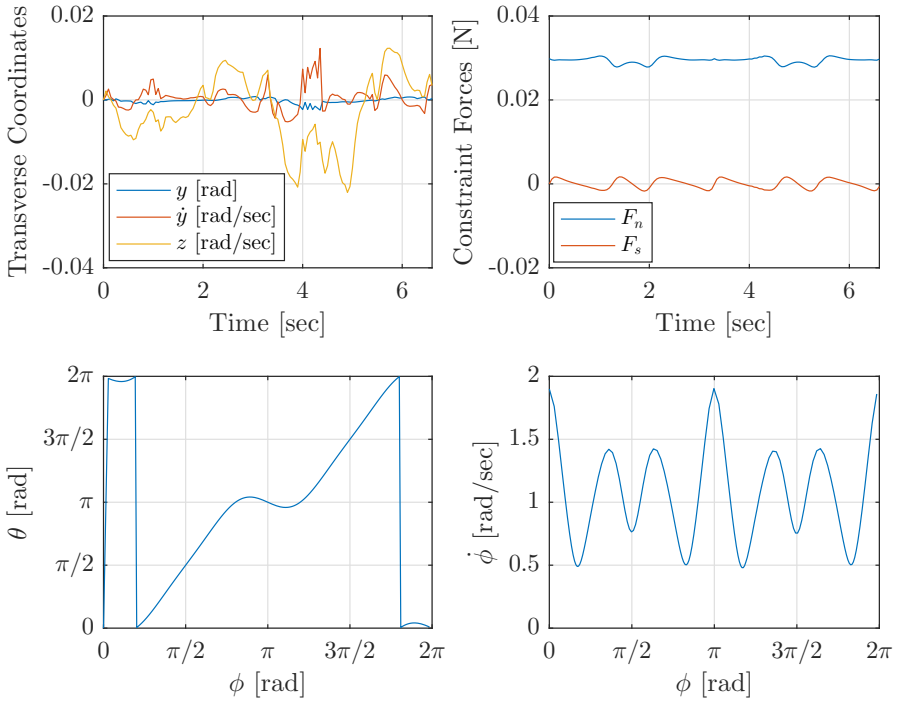

FIGURE 5.1: Simulation result when starting on the trajectory, i.e. initial condition 5.1. Upper Left: Transverse coordinates start and stay close to zero, implying that the periodic motion is performed properly. Upper Right: Normal force F_N is always positive showing that the ball will stay on the edges of the plates during the complete motion. Lower Left: VHC is satisfied. Lower Right: Phase portrait of $\varphi, \dot{\varphi}$ showing the designed periodic motion.

5.2 Region of Attraction of the Controlled Butterfly Robot

The trajectory designed in Chapter 3 is designed in such a way, that the angular velocity of the ball is always positive. However, in practice it is almost impossible to let the BR start with a correct initial velocity other than 0. This is one argument to investigate the region of attraction of the controlled BR. Another argument to find the region of attraction is that in practice it can happen that the actual trajectory deviates from the designed trajectory, for multiple reasons. Therefore, this section is dedicated to find a region of attraction by means of numerical simulations.

The simulations are performed for the model in excessive coordinates, 2.21, which gives insight in the constraint forces F_n and F_s. This allows for conclusions about feasibility of the motion. The region of attraction can be found by performing simulations with various initial conditions. The simulations shows whether the controlled BR is able to follow the periodic trajectory and keep the ball on the edges of the plates, when such a situation occurs during simulations/experiments. The initial conditions are chosen in a $M \times N \times N \times N, M = 5, N = 11$ grid as

$$\varphi_0 = \left[-\frac{\pi}{2}, -\frac{\pi}{4}, 0, \frac{\pi}{4}, \frac{\pi}{2}\right], \tag{5.2a}$$

$$\theta_0 = [-\pi, \pi], \tag{5.2b}$$

$$\dot{\varphi}_0 = [-10, 10], \tag{5.2c}$$

$$\dot{\theta}_0 = [-10, 10]. \tag{5.2d}$$

The initial conditions for φ_0 are chosen this way because of the symmetry in the BR. The results will be similar for $\varphi_0 + \pi$.

The motion is classified as feasible when the transverse coordinates go to zero and the condition on the normal force F_n is satisfied in a 10 seconds simulation. The results are visualized in a series

of three dimensional plots over the coordinate φ, see Figure 5.2. The filled black dots represent feasible initial conditions, while the transparent dots represent non-feasible initial conditions.

Even thought the figure is dense populated, some conclusions can be drawn. The most important conclusion about these results is that there is a region of attraction, which is larger than only the designed periodic trajectory. This allows for some deviation from the nominal trajectory. An observation is that the region of attraction changes with φ, which is expected due to the shape of the BR. Furthermore, it can be concluded that for $q_0 = 0$, the BR is able to start up and perform the task. This is a convenient initial condition in practice. Note that these results are, among others, based on the desired trajectory, choice of transverse coordinates and the LQR weighting matrices. If one of the aforementioned components is changed, the region of attraction changes as well.

5.3 Summary

This chapter showed that the controlled BR is able to perform the task of continuous one-directional rollings of the ball when starting on the designed trajectory. Furthermore, a region of attraction is presented visually, which shows that the BR is capable of converging to the designed trajectory up to a certain level of deviations. Here, it was also observed that the region of attraction changes for different positions of the ball φ. Another result is that the BR is able to start from a zero velocity and position, which is convenient for conducting experiments. The results are not tested on a practical setup, since there was no available.

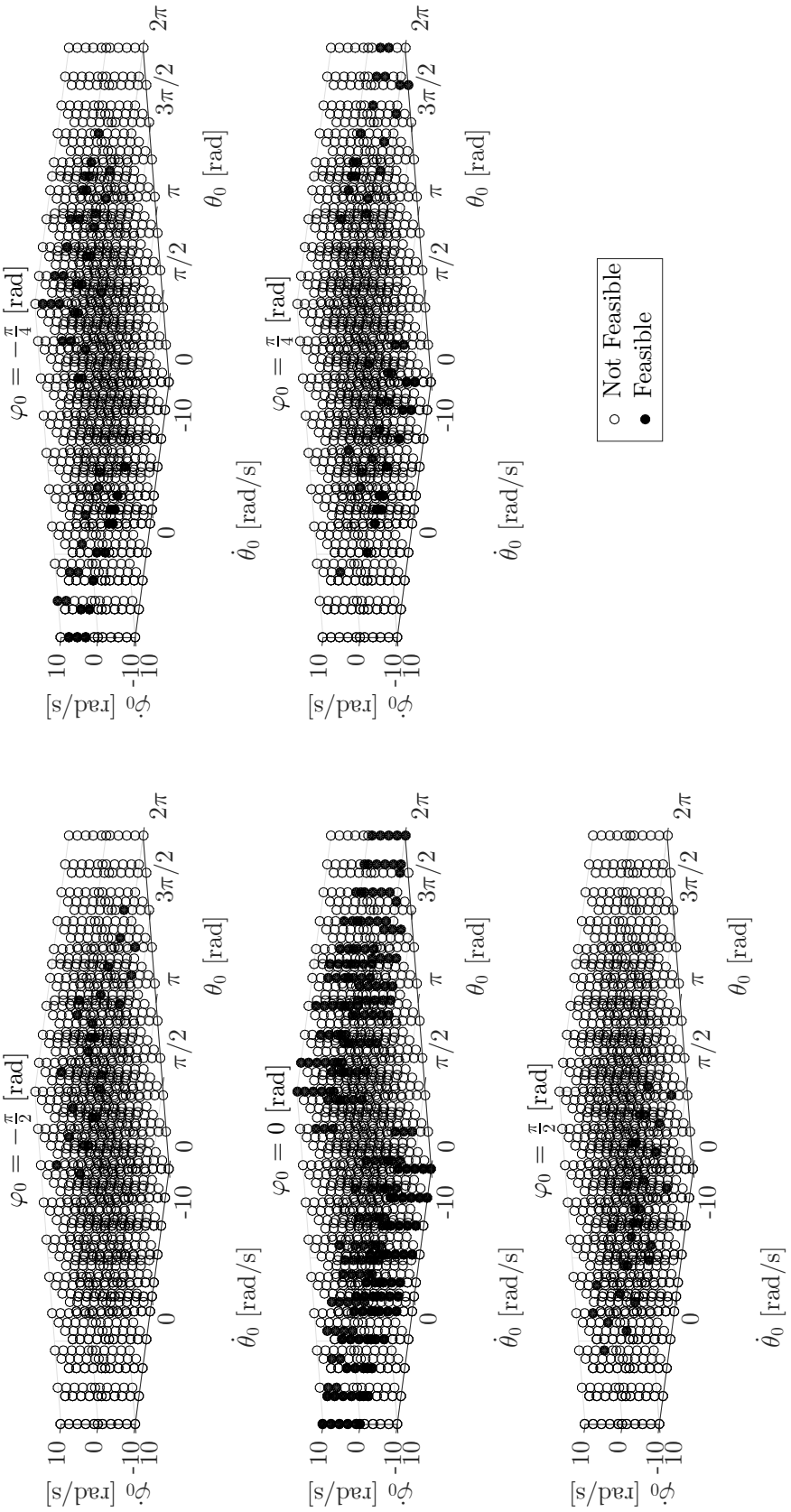

FIGURE 5.2: Region of attraction given for $\varphi = \left[-\frac{\pi}{2}, -\frac{\pi}{4}, 0, \frac{\pi}{4}, \frac{\pi}{2}\right]$. The black filled circles show feasible initial conditions, while the transparent circles show infeasible initial conditions.

Chapter 6

Conclusions & recommendations

This report presents an approach to design a controller which allows the Butterfly Robot (BR) to perform the task of rolling the ball continuously in one direction on the edge of the plates. First of all, the dynamics of the BR are derived using a Lagrangian approach. The constraints here are that the ball is always in point contact with each of the plates and that the ball rolls without slipping. This results in a model in excessive coordinates, which gives insight in the constraint forces, and a model in generalized coordinates, which is further used for tasks as motion planning and orbital stabilization.

The next step is to find a feasible periodic motion for the BR. Hereto, the approach of Virtual Holonomic Constraints (VHC) is used. After such a VHC is introduced, the reduced dynamics are written in only one degree of freedom. The desired trajectory is planned by considering the zero dynamics of the reduced system. Furthermore, the control input providing invariance is found using the reduced dynamics. However, this motion appears to be unstable and needs to be stabilized.

The method of orbital stabilizing is used to find a stabilizing feedback controller. This method is based on the derivation and linearization of the transverse dynamics in a vicinity of the nominal orbit. Stability of the origin of the linearized transverse dynamics is equivalent to exponential orbital stability of designed trajectory. An LQR method is used for which a periodic differential Riccati equation is solved using a convex approximation approach. The control law consists of a part ensuring the VHC and a part stabilizing the periodic motion.

Finally, a numerical analysis is performed. Starting on the designed trajectory, the BR is able to perform the task of continuous one-directional rollings of the ball. Furthermore, a region of attraction is given, which shows that the BR is capable of converging to the designed trajectory up to a certain level of deviations. It is also observed that the region of attraction changes for different positions of the ball. Another result is that the BR is able to start from a zero velocity and position, which is convenient for conducting experiments. The results are not tested on a practical setup, since there was no available.

A recommendation is to implemented the results given in this result on a physical setup. Now, all the conclusions are based on numerical simulations. Ideally, the controlled BR in practice would give a verification of the conclusions in this report.

It is recommended to conduct research for the model dependent transverse coordinate. The method described in this report uses the model to calculate the third transverse coordinate. However, if the model is not accurate enough, this could lead to a different trajectory, which might not be desired. Therefore, it is preferred to have all the coordinates model independent. Research should show whether it is possible to find such a set of coordinates.

Another recommendation is to exploit the work on finding a state feedback law for the linear time varying system resulting from transverse linearization using a Periodic Quadratic Lyapunov. It

is known that such a Lyapunov function exists, since any stable periodic LTV system possesses such a Lyapunov and this system is controllable, meaning that there exists a state feedback law ensuring stability. Finding such a Lyapunov function gives the possibility to compare the region of attraction of controllers obtained by different approaches. In order to find the Lyapunov function, a relaxation can be applied which should ensure a decrease in the Lyapunov function over a period instead of decreasing at all times.

Appendix A

Lyapunov Approach for Designing a Stabilizing State Feedback

One way of assessing stability for a (non)linear system, is the so called Lyapunov's method for stability. A linear time-invariant (LTI) system is exponentially stable if a function $V(\xi)$ can be found for which holds:

- $V(\xi) = 0$ if $\xi = 0$,
- $V(\xi) > 0$ if $\xi \neq 0$,
- $\dot{V}(\xi) = 0$ if $\xi = 0$,
- $\dot{V}(\xi) < 0$ if $\xi \neq 0$.

For a stable LTI system, there exists always a quadratic Lyapunov function [12], i.e.

$$V(\xi) = \xi^\top P \xi, \quad P \succ 0,$$

proving stability. For stable periodic Linear Time Varying (LTV) system, there exists always a periodic time-varying quadratic Lyapunov function [12], i.e.

$$V(\xi) = \xi^\top P(t) \xi, \quad P(t) = P(t+T) \succ 0, \quad t \in [0, T), \tag{A.1}$$

proving stability. This result can be used to shape a state feedback controller for the LTV system in 4.11.

Introducing a periodic Lyapunov function as A.1, the time derivative can be found as

$$\dot{V} = \dot{\xi}(t)^\top P(t) \xi(t) + \xi(t)^\top \dot{P}(t) \xi(t) + \xi(t)^\top P(t) \dot{\xi}(t).$$

For stability it is sufficient that the Lyapunov function decreases at any time, i.e. $\dot{V} < 0 \, \forall \, t \in [0, T)$ or on matrix level

$$(A(t) - B(t)K(t))^\top P(t) + \dot{P}(t) + P(t)(A(t) - B(t)K(t)) \prec 0.$$

Pre- and postmultiplying with $P^{-1}(t)$ leaves

$$P^{-1}(t) \left(A(t) - B(t)K(t)\right)^\top + P^{-1}(t)\dot{P}(t)P^{-1}(t) + (A(t) - B(t)K(t))P^{-1}(t) \prec 0$$
$$P^{-1}(t)A(t)^\top - P^{-1}(t)K^\top(t)B^\top(t) + P^{-1}(t)\dot{P}(t)P^{-1}(t) + A(t)P^{-1}(t) - B(t)K(t)P^{-1}(t) \prec 0.$$

Now apply a Schur complement to obtain

$$\begin{bmatrix} P^{-1}(t)A(t)^\top - P^{-1}(t)K^\top(t)B^\top(t) + A(t)P^{-1}(t) - B(t)K(t)P^{-1}(t) & P^{-1}(t) \\ P^{-1}(t) & -\dot{P}^{-1}(t) \end{bmatrix} \prec 0.$$

Introduce the linearizing variables $X(t) = P^{-1}(t), \dot{X}(t) = \dot{P}^{-1}(t)$ and $Y(t) = K(t)P^{-1}(t)$, which leads to the LMI

$$\begin{bmatrix} X(t)A^\top(t) - Y^\top(t)B^\top(t) + A(t)X(t) - B(t)Y(t) & X(t) \\ X(t) & -\dot{X}(t) \end{bmatrix} \prec 0. \tag{A.2}$$

As was done for the solution of the PDRE, the solution $X(t)$ can be also approximated by a truncated series of the form

$$\tilde{X}(t) = \sum_{k=-M}^{M} e^{i\omega tk} X_k \text{ and } \dot{\tilde{X}}(t) = \sum_{k=-M}^{M} i\omega k e^{i\omega tk} X_k,$$

with X_{-k} being the complex conjugate of X_k.

If the time horizon is divided into N points within the period $[0, T)$, then the LMIs are given by $\tilde{X}(t) \succ 0$ and A.2 $\forall\, t_i,\, i = 0, 1, \ldots, N$. However, Matlab runs into numerical problems when trying to solve this problem. This is most likely because of the conservativeness of the formulated problem. It is not necessary that $\dot{V}(\xi)$ decreases at every time moment. It is necessary and sufficient that $\dot{V}(\xi)$ decreases over a period, see Figure A.1 for an illustration. Due to time restrictions, the challenge of taking this relaxation into account is not further elaborated.

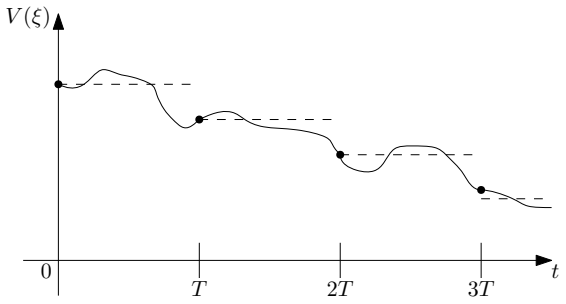

FIGURE A.1: Illustration showing that $V(\xi)$ only has to decrease over a period.

Bibliography

[1] KM. Lynch, N. Shiroma, H. Arai, K. Tanie. The roles of shape and motion in dynamic manipulation: the butterfly example. *in the Proceedings of the IEEE International Conference on Robotics and Automation (ICRA)*, 1998.

[2] H.M. Francke. Motion planning and analysis of the underactuated "Butterfly" robot. *University of Technology, Eindhoven, Netherlands, DC 2015.092*, 2015.

[3] S.J.A.M. van den Eijnden. Orbital stabilization and robustness analysis of the Butterfly robot with pre-defined periodic trajectories. *University of Technology, Eindhoven, Netherlands, DC 2015.093*, 2015.

[4] Joris Knol. The Butterfly-robot: theoretical behaviour of small perturbations and their effect on stability. *University of Technology, Eindhoven, Netherlands, DC 2016.041*, 2016.

[5] Maksim Surov, Anton Shiriaev, Leonid Freidovich, Sergei Gusev, Leonid Paramonov. Case study in non-prehensile manipulation: planning and orbital stabilization of one-directional rollings for the "Butterfly" robot. *IEEE International Conference on Robotics and Automation*, pages 1484–1489, 2015.

[6] Sergei V. Gusev, Anton S. Shiriaev, Leonid B. Freidovich. SDP-based approximation of stabilising solutions for periodic matrix Riccati differential equations. *International Journal of Control*, pages 1396–1405, 2016.

[7] N. van de Wouw. Multibody and Nonlinear dynamics: Lecture Notes and Exercises for the part on Multibody Dynamics 2015. *CIP-DATA LIBRARY TECHNISCHE UNIVERSITEIT EINDHOVEN*, 2013.

[8] Anton Shiriaev,John W. Perram,Carlos Canudas-de-Wit. Constructive tool for orbital stabilization of underactuated nonlinear systems: Virtual constraints approach. *IEEE TRANSACTIONS ON AUTOMATIC CONTROL*, 50:1164–1176, 2005.

[9] Anton S. Shiriaev, Leonid B. Freidovich, Ian R. Manchester. Can we make a robot ballerina perform a pirouette? orbital stabilization of periodic motions of underactuated mechanical systems. *IEEE International Conference on Robotics and Automation*, 32:200–211, 2008.

[10] Anton Shiriaev,Leonid B. Freidovich,Sergei Gusev. Transverse linearization for mechanical systems with several passive degrees of freedom with application to orbital stabilization. *American Control Conference*, 50:3039–329, 2009.

[11] Sergei Gusev, Stefan Johansson, Bo Kågström, Anton Shiriaev, Andras Varga. A numerical evaluation of solvers for the periodic riccati differential equation. *BIT Numerical Mathematics*, 50:301–329, 2010.

[12] Hassan K. Khalil. *Nonlinear Systems*. Prentice Hall, third edition edition, 2002.